Supplementary Information

Effect of proton sources on the electrocatalytic hydrogen evolution reaction mediated by a copper complex of bistriazolylpyridine

Gui-Shan Chen,[a] Chang Liu,[a] Xing-Jin Yang,[a] Zhi-Hao Zhan,[a] Tian-Shun Wang[a,b] and Hua-Xin Zhang[a,*]

[a]*School of Chemistry and Chemical Engineering, Guangxi University, No. 100, Daxue East Road, Nanning 530004, Guangxi, China*

[b]*Research Institute of Agro-Products Quality Safety and Testing Technology, Guangxi Academy of Agriculture Science, Nanning 530007, Guangxi, China*

[*] Corresponding author.
E-mail address: zhanghx@gxu.edu.cn (H.-X. Zhang).

Physical Measurements

The UV-Vis absorption spectra were recorded with Shimadzu UV2600 spectrophotometer. Infrared spectra were measured using the Perkin Elmer Frontier FT-IR spectrometer. ^{1}H and ^{13}C NMR spectra were obtained using the AVANCE III HD500 spectrometer. Elementary analyses (C, H, N) were performed on a Perkin–Elmer model 240C automatic instrument. SEM images were observed with a Hitachi S-4800 field emission scanning electron microscope and the EDS data were obtained with an X-Max Extreme spectrometer. Mass spectrometric analyses were conducted using an Agilent 1260-6545LC-Q-TOF mass spectroscopy with a positive-ion electrospray ionization mode. The powder X-ray diffraction (PXRD) data were measured using a Rigaku D/MAX 2500 V diffractometer. The X-ray photoelectron spectroscopy (XPS) data and the valence states of the metal elements were probed using a Thermo Scientific Nexsa instrument.

Crystal structure determination

A single crystal of Cudbes was mounted on a glass fibre and measured using graphite monochrome Mo-K_α radiation (λ = 0.71073 Å) on an Enraf-Nonius single crystal CAD-4 diffractometer. The data were collected at a temperature of 296 K with a maximum 2θ value of 51.58 for Cudbes. Experience absorption correction is applied using the SADABS program.[1] The structure was solved by direct method and refined by full-matrix least square method on F^2 using SHELXTL program.[2] ORTEP was used to draw the molecular structure.[3] CCDC2339302 contains the supplementary crystallographic data for Cudbes.

Electrochemical measurements

Electrochemical measurements were carried out in an airtight H-shaped electrochemical cell using a potentiostat CHI760E with a glassy carbon (GC) working electrode (diameter: 3.0 mm) at room temperature. Pt mesh is used as the counter electrode. Ag pseudo-reference electrode is a silver wire immersed in electrolyte solutions (0.1 M $TBAPF_6$ and 0.01 M $AgNO_3$ solutions) and separated from other electrodes by Vycor glass. The Fc^+/Fc^0 ($E_{1/2}$ = 0.09 V) was used as an internal reference electrode. Anhydrous 0.1 M $TBAPF_6$ CH_3CN solution was used as an electrolyte in all measurements. The concentration of the complex was 0 - 1.0 mM. The peak potential of irreversible redox process was determined by differential pulse voltammetry

All controlled potential electrolysis (CPE) experiments were carried out in an inert atmosphere with membrane-separated, gas-tight two-compartment glass cells. Experiments were conducted

using a potentiostat CHI760E with a GC working electrode (diameter: 6.0 mm). Pt mesh was used as the counter electrode. The potential was recorded with respect to the Ag pseudo-reference electrode (0.1 M $TBAPF_6$ and 0.01 M $AgNO_3$ solution).

The Faradaic efficiency was determined from the calibration curve derived from the H_2 gas standard and further quantified by gas chromatography on the Fuli 9790II instrument equipped with a 5 Å molecular sieve column, thermal conductivity detector and argon carrier gas.

Determination of the overpotential (η) and the Faradaic efficiency (FE)

The overpotential (η) was calculated according to Eq. S1.[4] Where $E_{cat/2}$ is the catalytic half-wave potential, E_{HA}^0 can be calculated by the Nernst equation as shown in Eq. S2. $E°_{H^+}$ is the electrode potential of the standard hydrogen electrode (H^+/H_2), which is -0.028 V in acetonitrile,[5] and pK_a is the dissociation constant in a given acid solution.

$$\eta = |E_{cat/2} - E_{HA}^0| \qquad (S1)$$

$$E_{HA}^0 = E°_{H^+} - (2.303RT/F)pK_a = -0.028 - 0.0591 \times pK_a \qquad (S2)$$

Using the values $pK_{a,AcOH}$ = 22.3, $pK_{a,TFA}$ = 12.7 and $pK_{a,TsOH}$ = 8.7, the thermodynamic potential $E°_{AcOH}$ is calculated to be -1.35 V, $E°_{TFA}$ is calculated to be -0.78 V, and $E°_{TsOH}$ is calculated to be -0.54 V.

In the CPE experiments, the Faradaic efficiency (FE) of the HER catalyzed by Cudbes was calculated by Eq. S3.[6]

$$\text{Faradaic efficiency} = zn_{H_2}F/Q \times 100\ \% \qquad (S3)$$

Where n_{H_2} represents the number of moles of H_2 generated during electrolysis, z represents the number of electrons per mole of H_2 (= 2), F represents the Faraday constant (= 96500) and Q represents the total amount of charge accumulated during one hour electrocatalysis.

Table Sl Crystallographic data and structural refinement parameters for Cudbes.

Complex	Cudbes
Empirical formula	$C_{30}H_{30}Cl_2CuN_{14}O_{16}$
Formula weight	977.12
Temperature / K	296(2)
Crystal system	monoclinic
Space group	*P*2(1)/n
a /Å	22.155(3)
b /Å	12.3764(17)
c /Å	30.424(4)
Z	8
α / °	90
β / °	102.455(3)
γ / °	90
Crystal size / mM	0.23 × 0.20 × 0.15
Absorption coefficient / mM^{-1}	0.756
h	$-26 \le h \le 27$
k	$-15 \le k \le 13$
l	$-37 \le l \le 37$
F(000)	3992
θ for data collection / °	1.371~25.788
Reflections collected / unique	19103 / 7445 [R(int) = 0.0253]
Data / restraints / parameters	7784 / 0 / 568
Goodness-of-fit on F^2	0.789
Final *R* indices [$I > 2\sigma(I)$]	$R_1 = 0.0549$， $wR_2 = 0.1707$

Table S2 Bond lengths (Å) and bond angles (°) for Cudbes .

Cu1-N1	2.006(3)	Cu1-N2	2.346(3)
Cu1-N5	2.280(3)	Cu1-N8	1.976(3)
Cu1-N9	2.104(3)	Cu1-N12	2.095(3)
N8-Cu1-N1	175.94(11)	N8-Cu1-N12	79.60(12)
N1-Cu1-N12	98.30(11)	N1-Cu1-N9	103.54(12)
N8-Cu1-N5	98.79(11)	N1-Cu1-N5	77.50(11)
N12-Cu1-N5	85.00(11)	N9-Cu1-N5	99.79(12)
N8-Cu1-N2	106.82(11)	N1-Cu1-N2	77.00(11)
N12-Cu1-N2	102.99(11)	N9-Cu1-N2	81.99(12)
N5-Cu1-N2	154.12(11)	N8-Cu1-N9	78.61(13)
N12-Cu1-N9	158.15(13)		

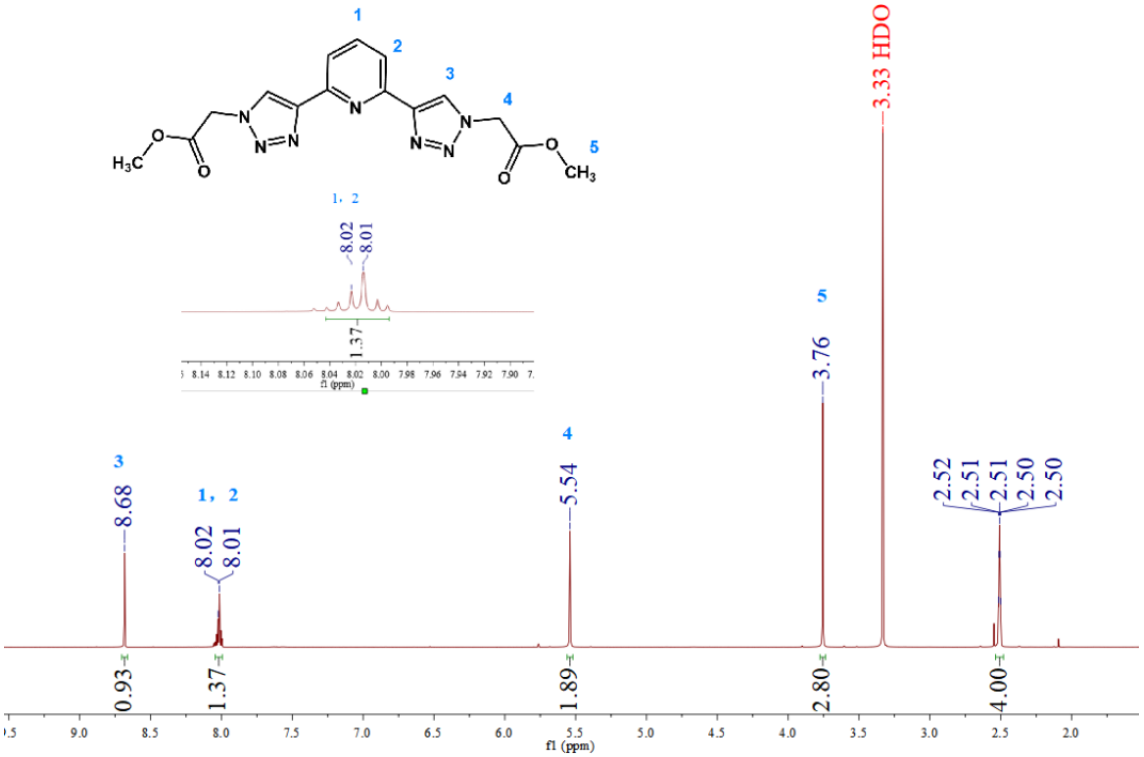

Fig. S1 ^{1}H NMR of dbes in $CDCl_3$

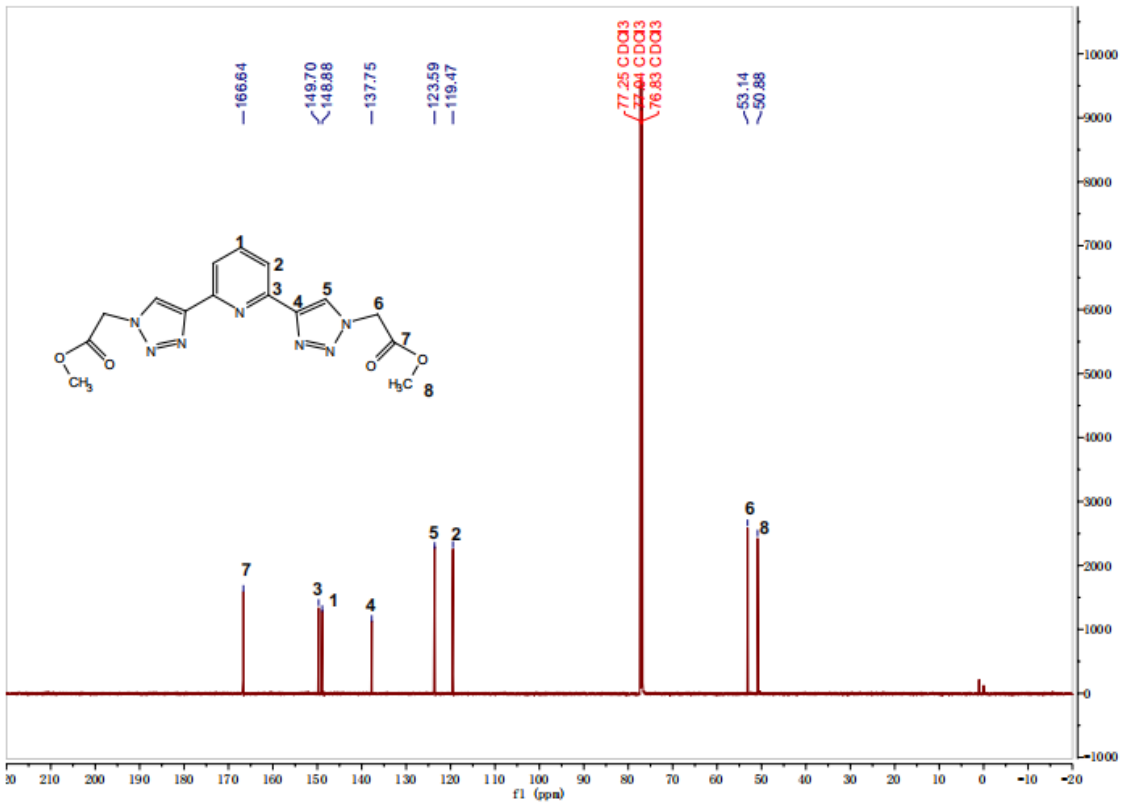

Fig. S2 ^{13}C NMR of dbes in $CDCl_3$

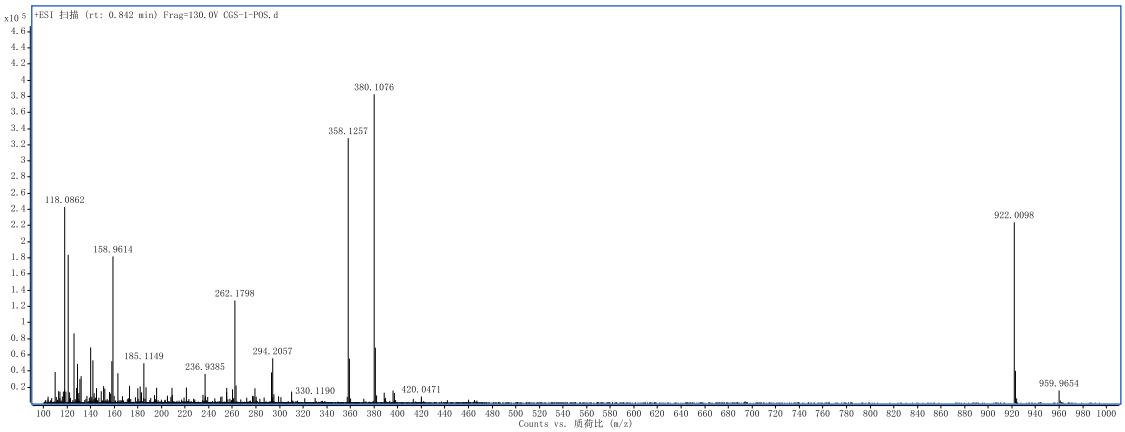
+ESI 扫描 (rt: 0.842 min) Frag=130.0V CGS-1-POS.d
380.1076
358.1257
118.0862
922.0098
158.9614
262.1798
185.1149
294.2057
236.9385
330.1190
420.0471
959.9654
Counts vs. 质荷比 (m/z)

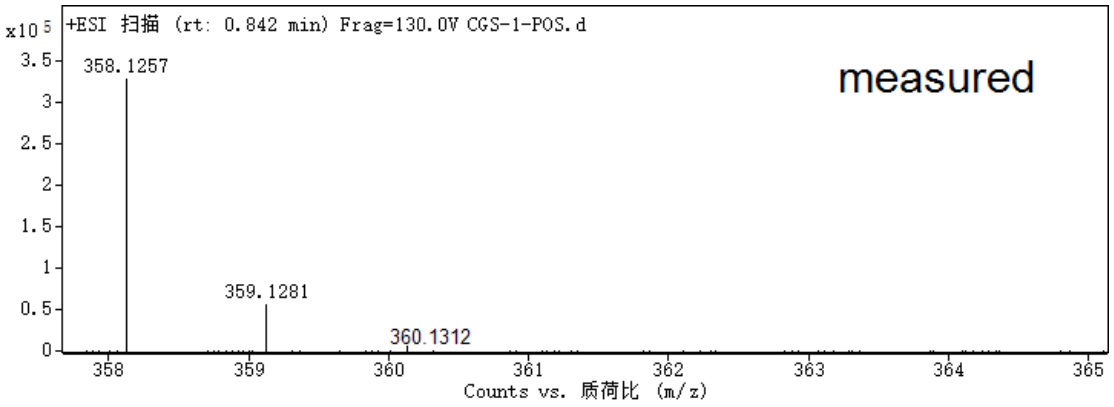
+ESI 扫描 (rt: 0.842 min) Frag=130.0V CGS-1-POS.d
measured
358.1257
359.1281
360.1312
Counts vs. 质荷比 (m/z)

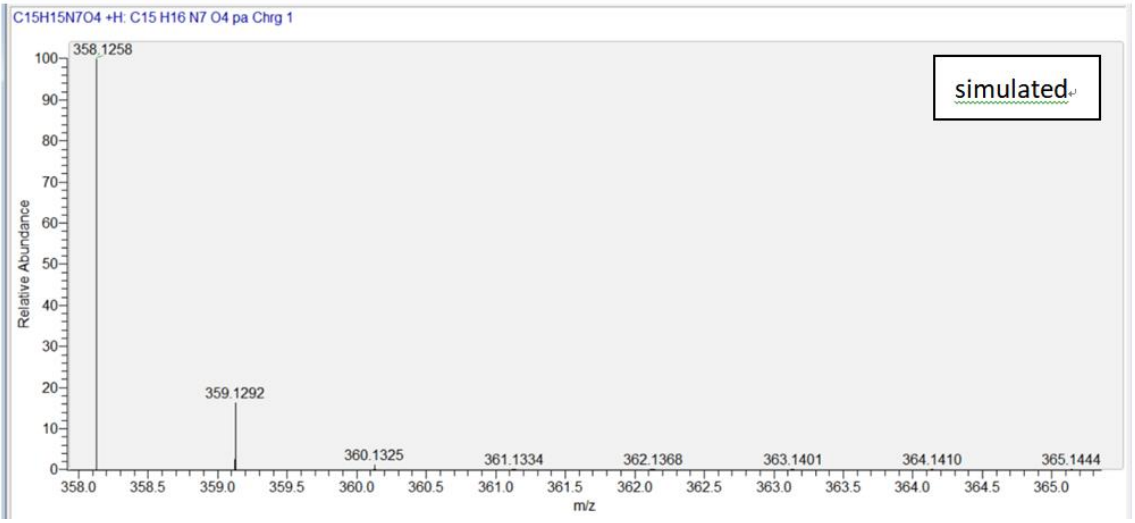
C15H15N7O4 +H: C15 H16 N7 O4 pa Chrg 1
simulated
358.1258
359.1292
360.1325
361.1334
362.1368
363.1401
364.1410
365.1444
Relative Abundance
m/z

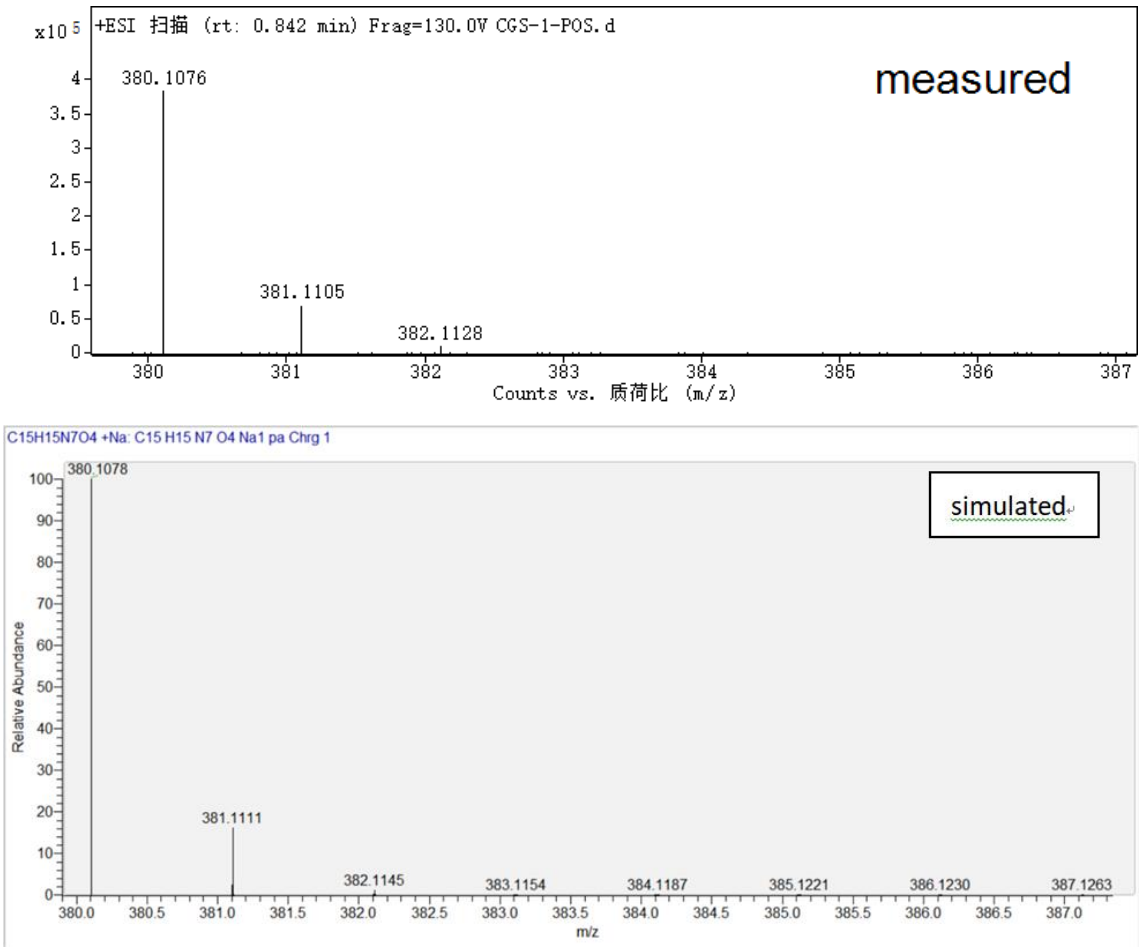

Fig. S3 Positive-ion electrospray ionization mass spectra (ESI-MS) of dbes in CH_3CN.

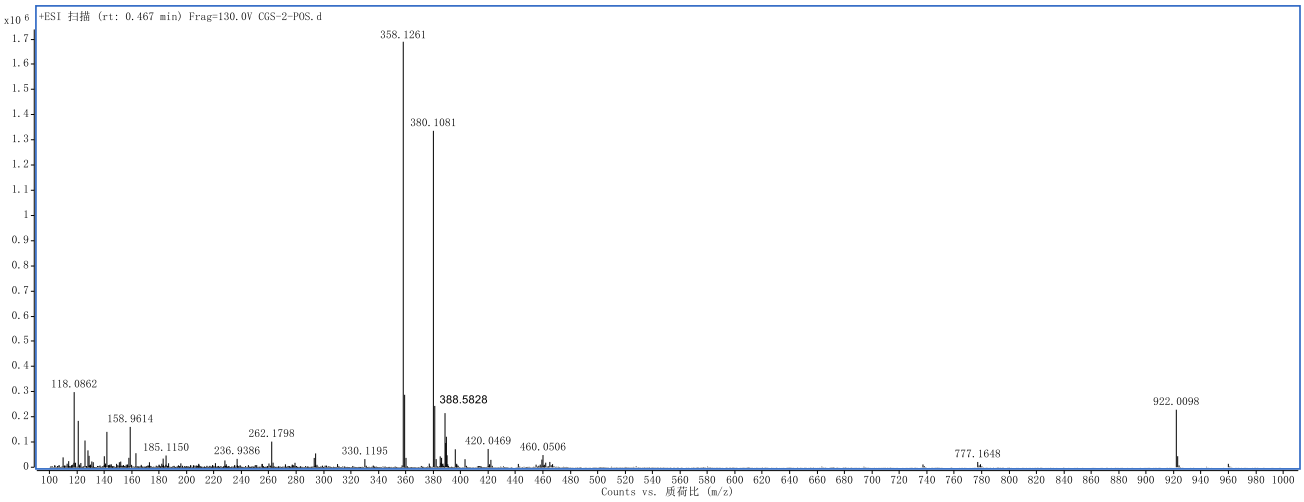

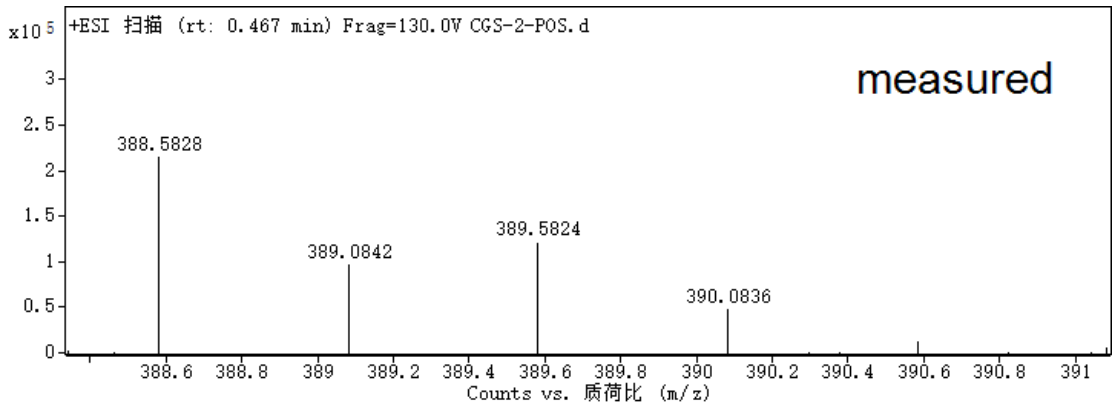
x10 5
+ESI 扫描 (rt: 0.467 min) Frag=130.0V CGS-2-POS.d
measured
388.5828
389.0842
389.5824
390.0836
Counts vs. 质荷比 (m/z)

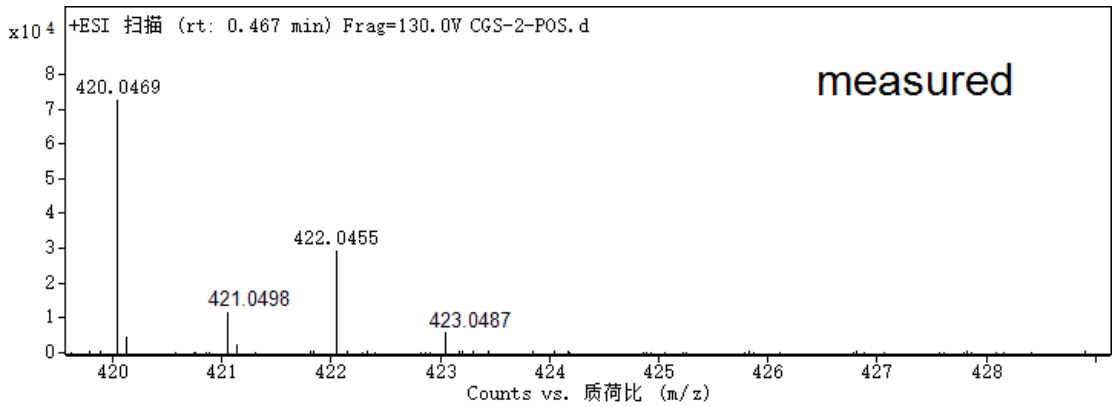
x10 4
+ESI 扫描 (rt: 0.467 min) Frag=130.0V CGS-2-POS.d
measured
420.0469
422.0455
421.0498
423.0487
Counts vs. 质荷比 (m/z)

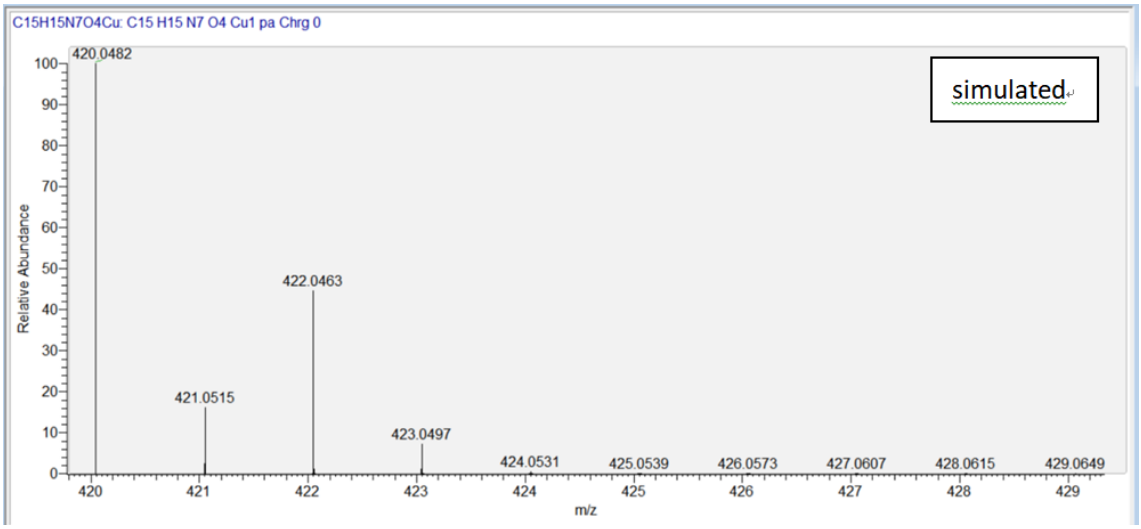
C15H15N7O4Cu: C15 H15 N7 O4 Cu1 pa Chrg 0
simulated
420.0482
422.0463
421.0515
423.0497
424.0531
425.0539
426.0573
427.0607
428.0615
429.0649
Relative Abundance
m/z

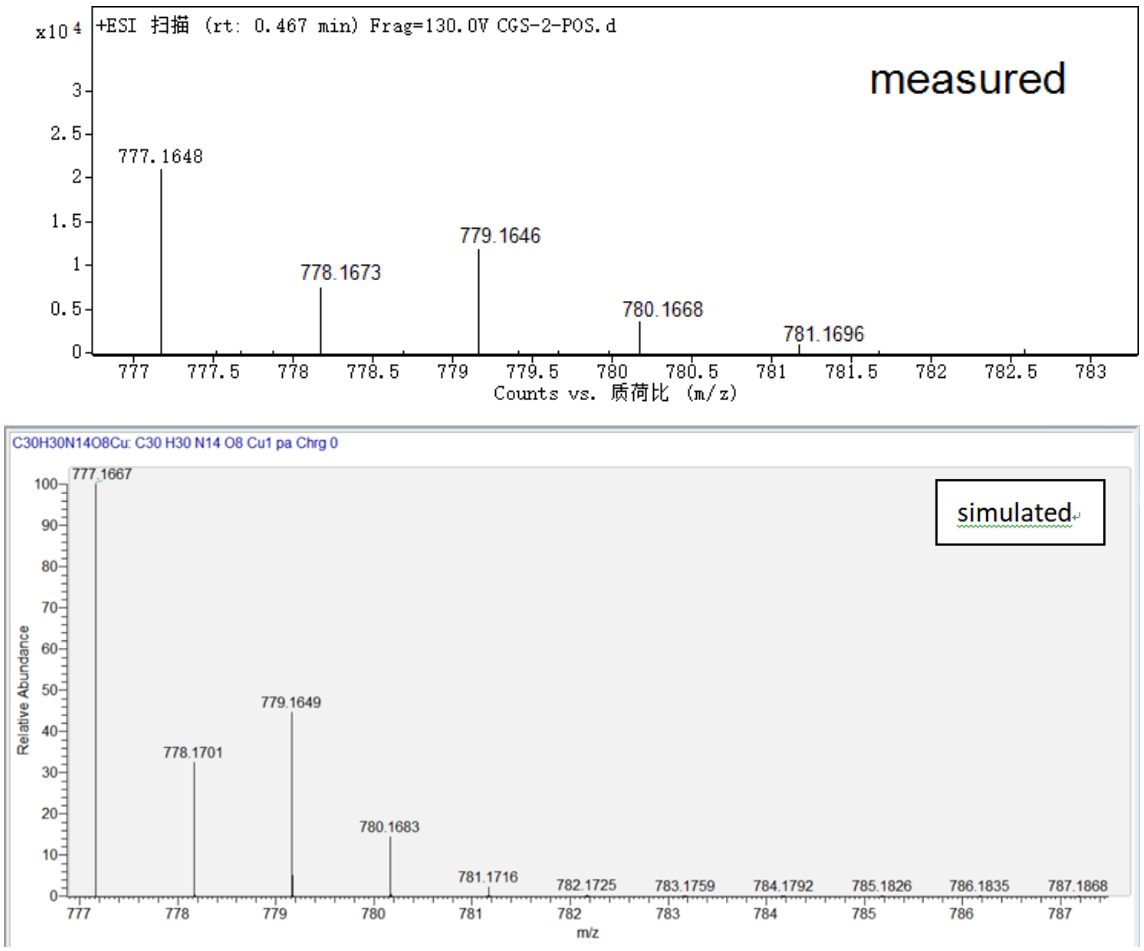

Fig. S4 Positive-ion electrospray ionization mass spectra (ESI-MS) of Cudbes in CH_3CN.

Table S3 ESI-MS data of dbes and Cudbes.

Fragment Species	Observed (calculated)
$\{dbes+H\}^+$	358.1257 (358.1258)
$\{dbes+Na\}^+$	380.1076 (380.1078)
$[Cu(dbes)_2]^{2+}$	388.5828 (388.5896)
$[Cu(dbes)-H]^+$	420.0469 (420.0482)
$[Cu(dbes)_2-H]^+$	777.1648 (777.1667)
$\{[Cu(dbes)]+TFA-H\}^+$	533.0325 (533.0332) (in Fig. S33)

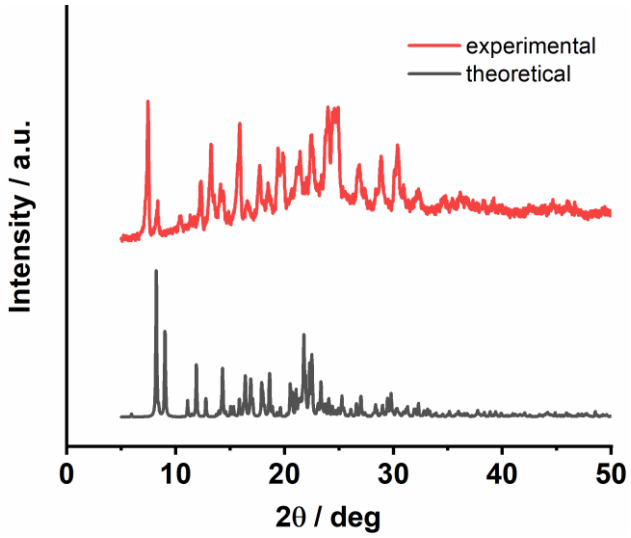

Fig. S5 Experimental and simulated powder X-ray diffraction (PXRD) patterns for Cudbes.

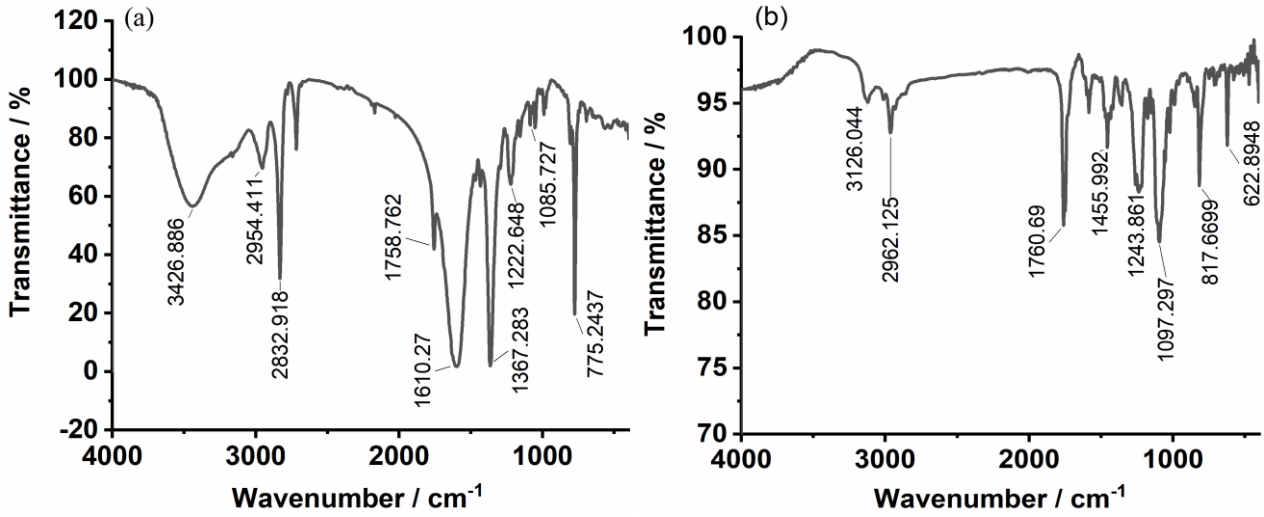

Fig. S6 IR spectra of (a) dbes and (b) Cudbes.

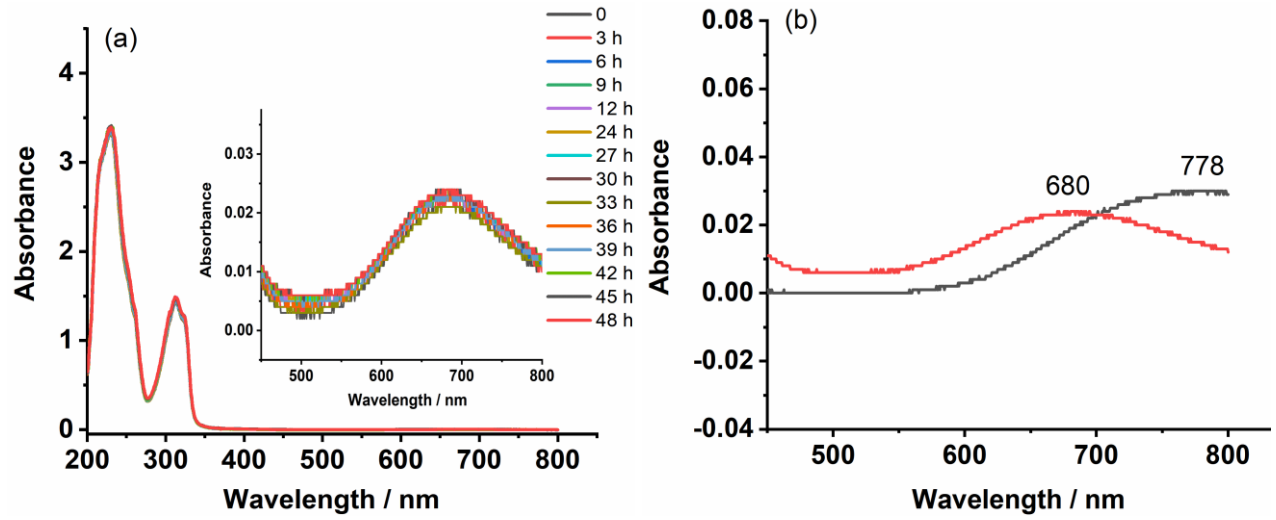

Fig. S7 UV-vis absorption spectra of (a) Cudbes in CH_3CN at different time, (b) $Cu(ClO_4)_2$ (black line) and Cudbes (red line) in CH_3CN after 48 h. Concentration: 0.1 mM.

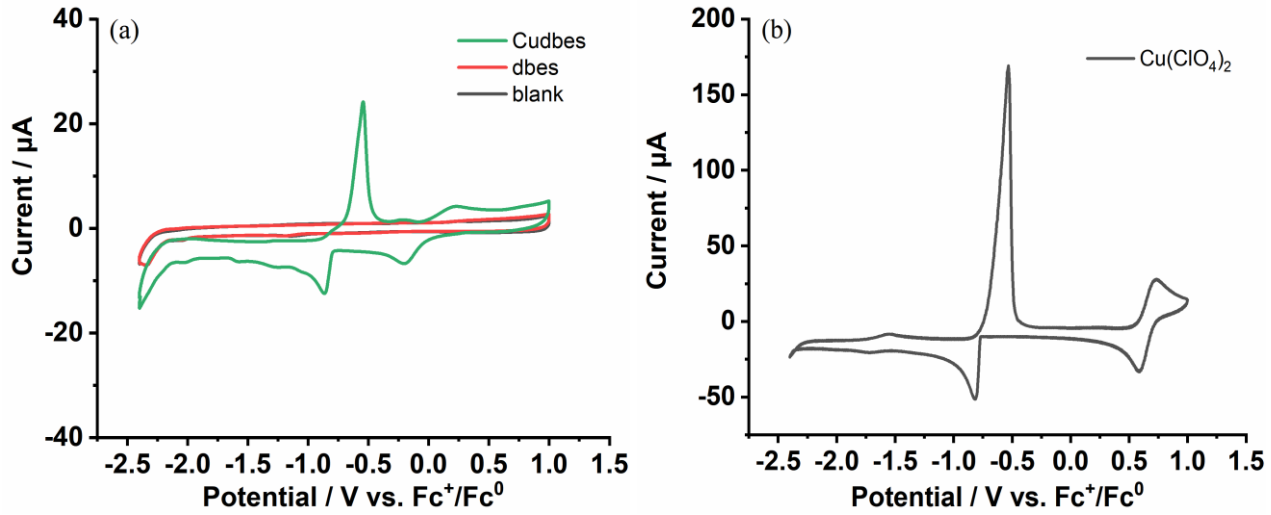

Fig. S8 Cyclic voltammograms using glassy carbon electrode in CH_3CN containing 0.1 M $TBAPF_6$ for (a) Cudbes, dbes and blank, (b) $Cu(C1O_4)_2$. Scan rate: 0.1 V s^{-1}. Concentration: 0.5 mM.

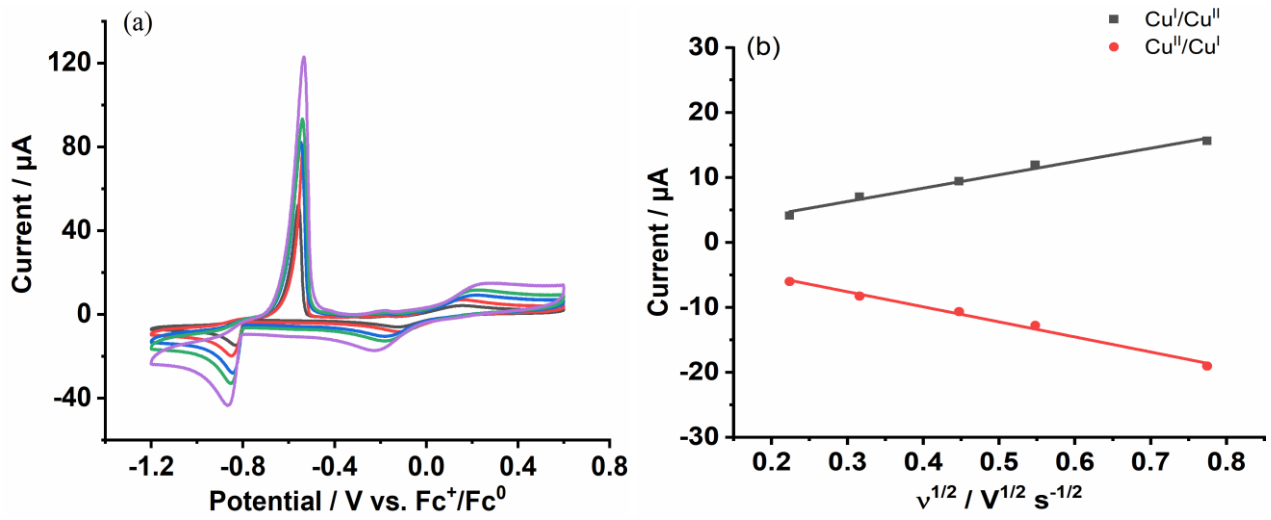

Fig. S9 (a) Cyclic voltammograms of 0.5 mM Cudbes in CH_3CN containing 0.1 M $TBAPF_6$ at scan rates of 0.05, 0.1, 0.2, 0.3 and 0.6 V s^{-1}. (b) Plots of the peak current (i_p) vs square root of scan rate.

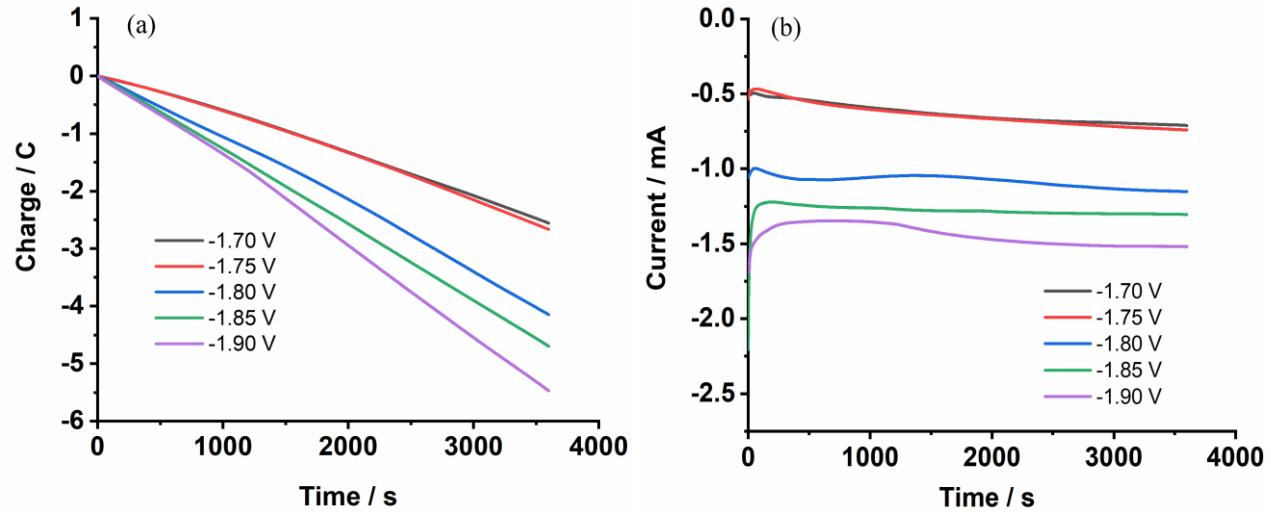

Fig. S10 (a) Charge-time curves and (b) current-time curves of 0.5 mM Cudbes in 0.1 M $TBAPF_6$ CH_3CN solution with 200 equivalents of AcOH during the electrolysis at -1.70 V, -1.75 V, -1.80 V, -1.85 V and -1.90 V. Glassy carbon working electrode.

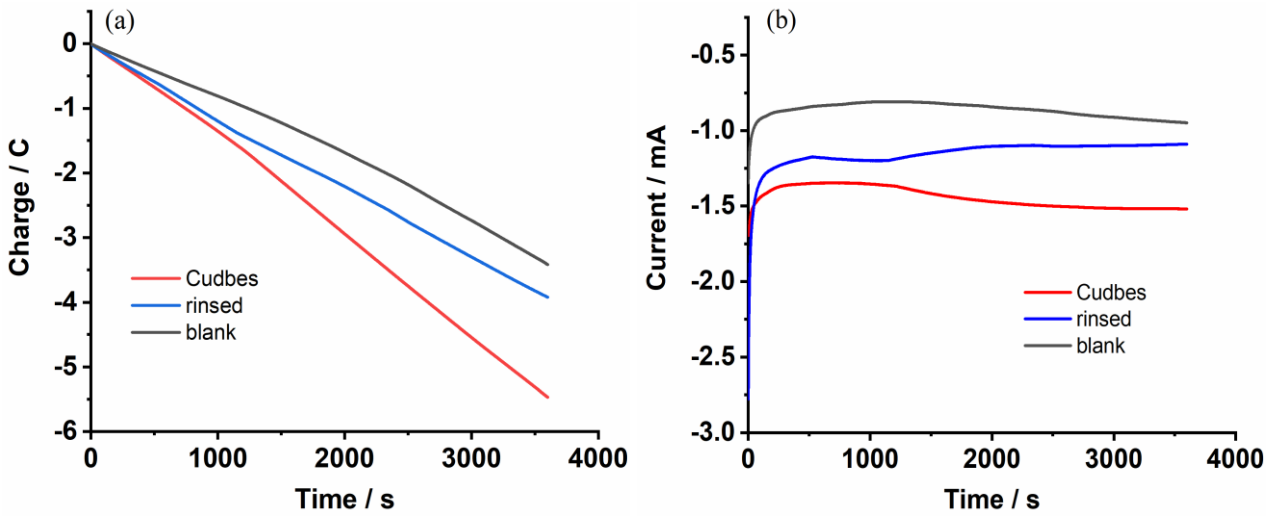

Fig. S11 (a) Charge-time curves and (b) current-time curves of 0.5 mM Cudbes in 0.1 M $TBAPF_6$ CH_3CN containing 200 equivalents of AcOH during the electrolysis at -1.90 V. Glassy carbon working electrode.

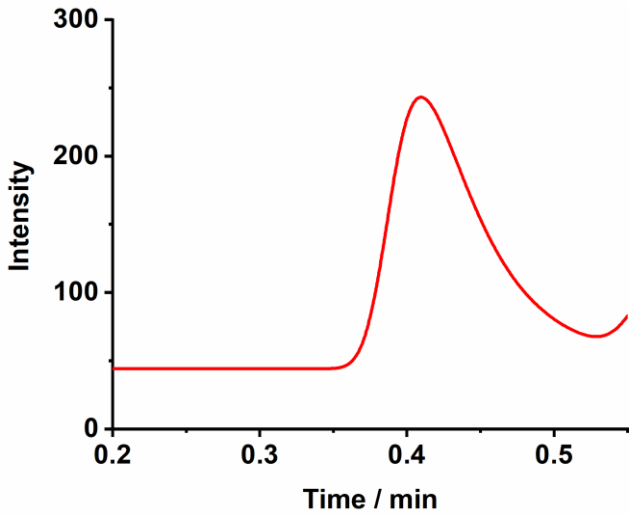

Fig. S12 Gas chromatographic spectrum of 0.5 mM Cudbes in 0.1 M $TBAPF_6$ CH_3CN containing 200 equivalents of AcOH after the electrolysis at -1.90 V for 1 h.

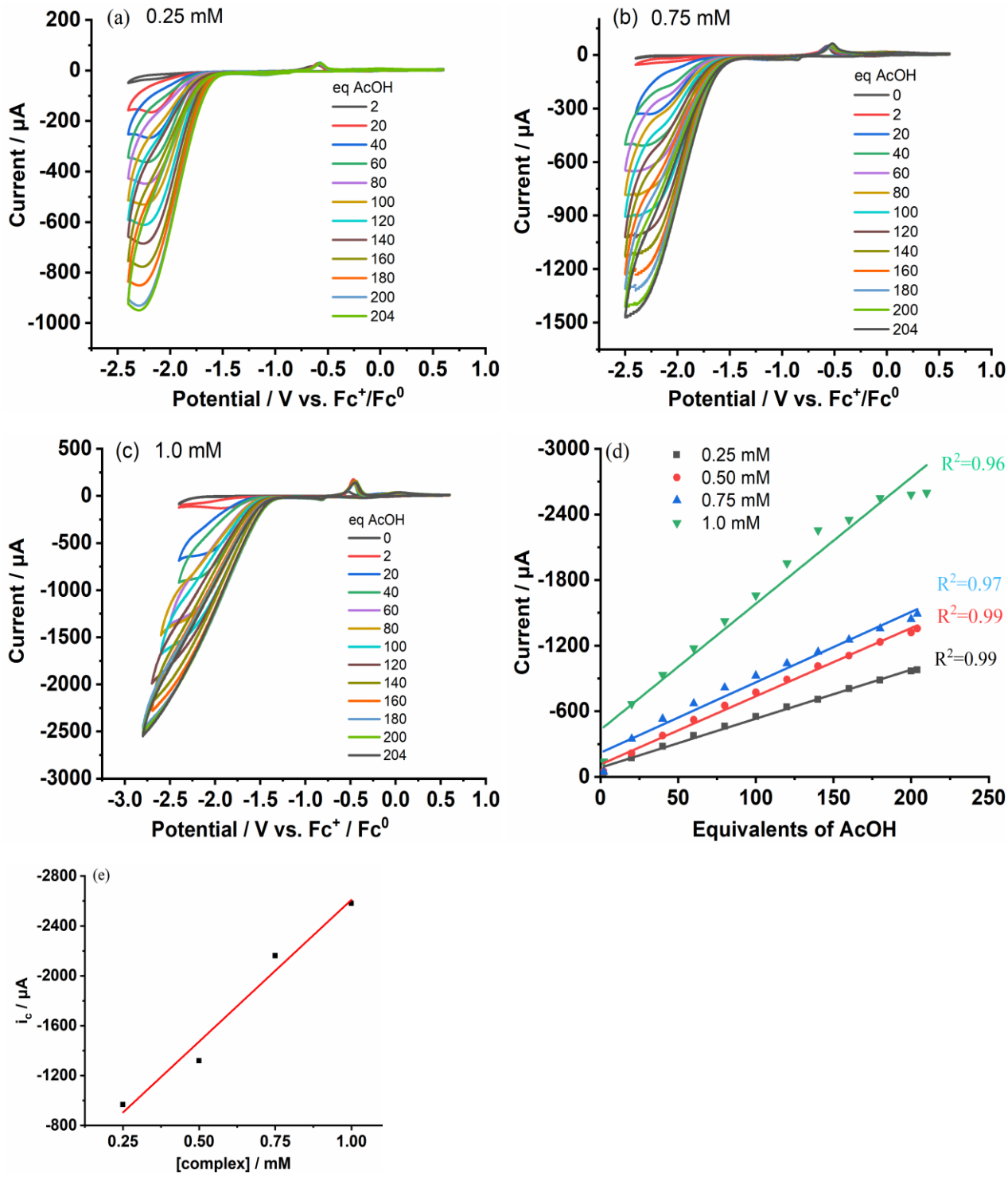

Fig. S13 Cyclic voltammograms in 0.1 M $TBAPF_6$ CH_3CN solutions with different concentrations of AcOH for (a) 0.25 mM Cudbes , (b) 0.75 mM Cudbes , (c) 1.0 mM Cudbes. (d) Plots of the catalytic currents (i_c) vs the concentration of AcOH. (e) Plots of the catalytic current (i_c) vs the concentration of Cudbes in the presence of 200 equivalents of AcOH. Glassy carbon working electrode, scan rate: 0.1 V s^{-1}.

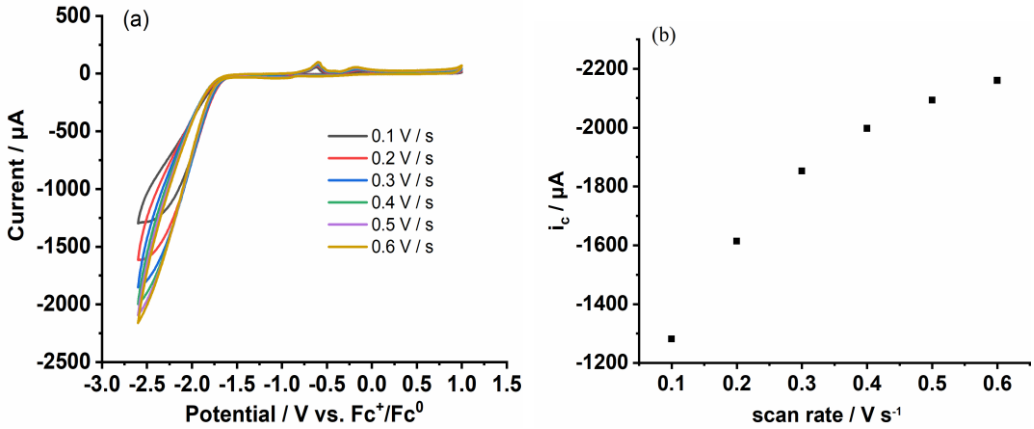

Fig. S14 (a) Cyclic voltammograms of 0.5 mM Cudbes in 0.1 M $TBAPF_6$ CH_3CN solution containing 200 equivalents of AcOH at scan rates of 0.1, 0.2, 0.3, 0.4, 0.5, and 0.6 V s^{-1}. (b) Plot of catalytic current (i_c) vs square root of scan rate. Glassy carbon working electrode.

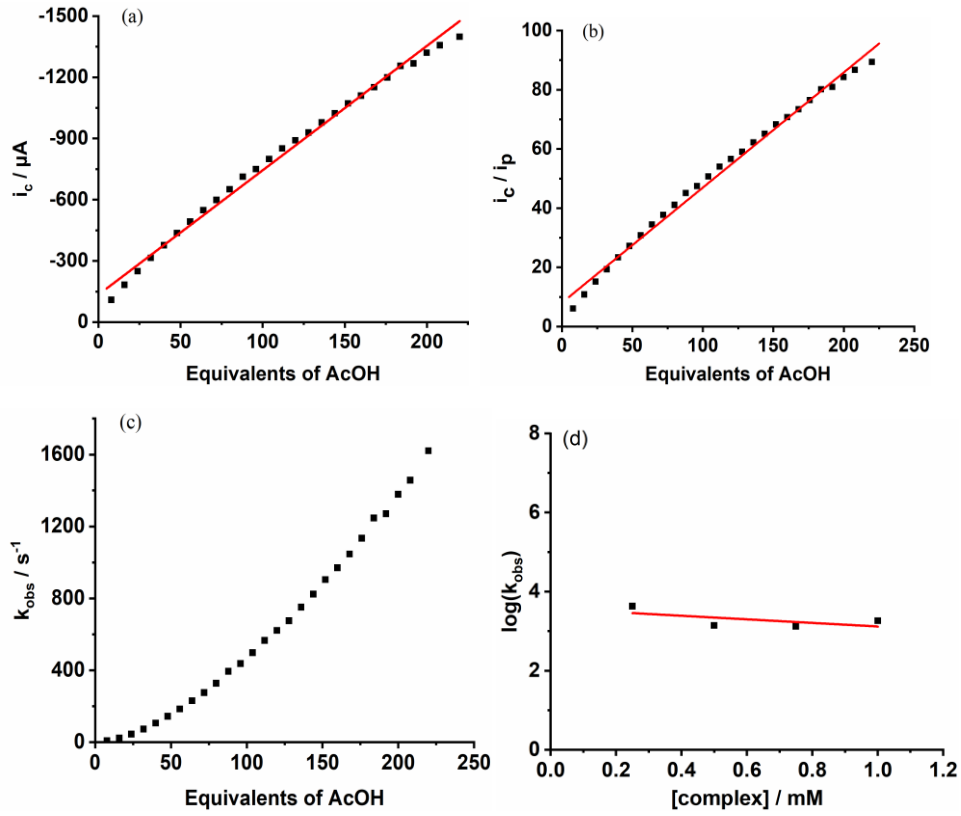

Fig. S15 (a) Plot of catalytic current (i_c) vs the concentration of AcOH. (b) Plot of i_c/i_p vs the concentration of AcOH. (c) Plot of k_{obs} vs the concentration of AcOH. Conditions: 0.5 mM Cudbes in 0.1 M $TBAPF_6$ CH_3CN solution, glassy carbon working electrode, scan rate: 0.1 V s^{-1}. (d) Plot of k_{obs} vs the concentration of Cudbes in the presence of 200 equivalents of AcOH. Concentration of Cudbes: 0.25 mM, 0.5 mM, 0.75 mM and 1.0 mM.

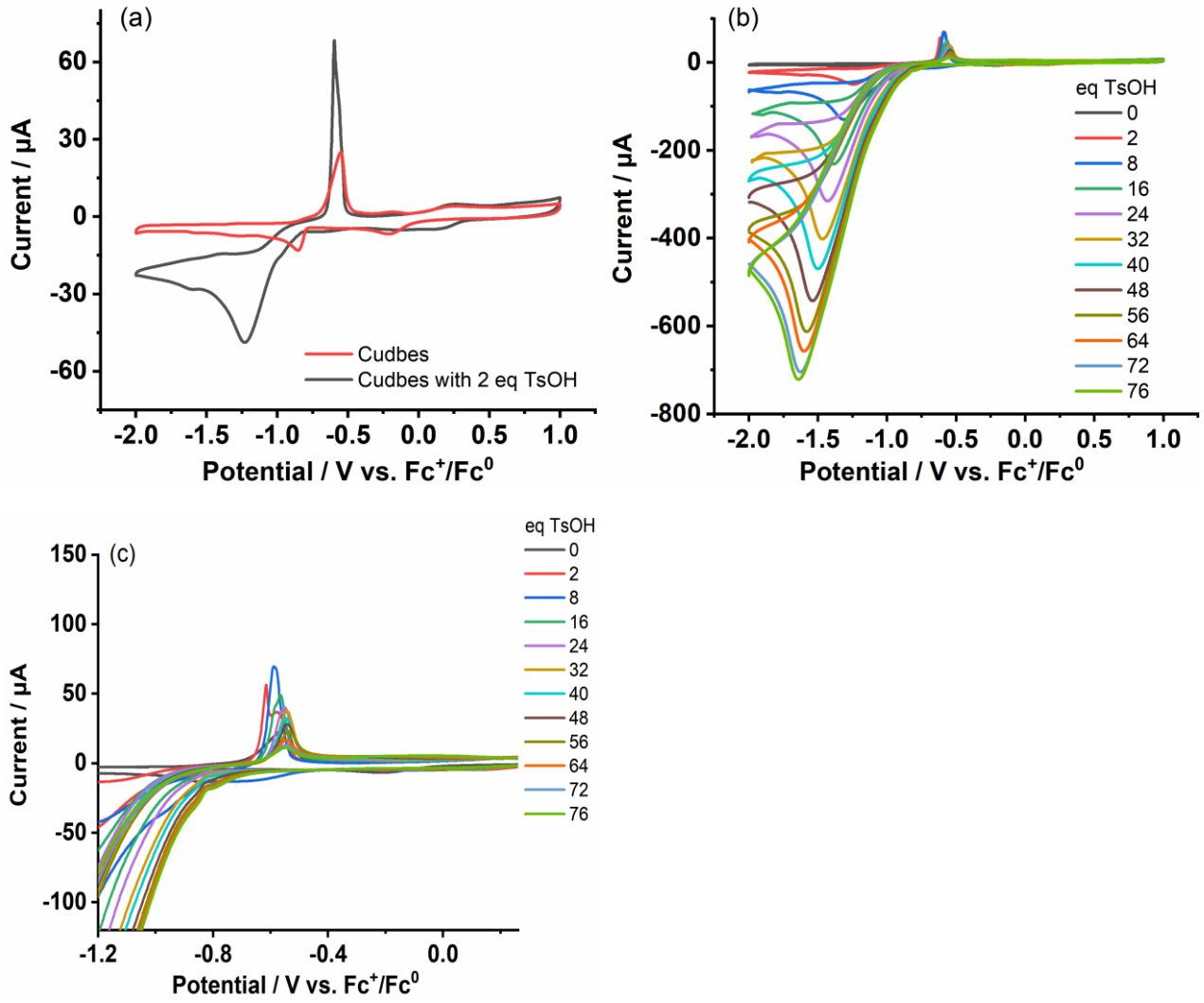

Fig. S16 Cyclic voltammograms of 0.5 mM Cudbes in 0.1 M $TBAPF_6$ CH_3CN solution: (a) with 2 equivalents of TsOH (black line) and without TsOH (red line), (b) with different concentrations of TsOH (0-76 equivalents), (c) Enlargement of Fig. (b). Glassy carbon working electrode, scan rate: 0.1 V s^{-1}.

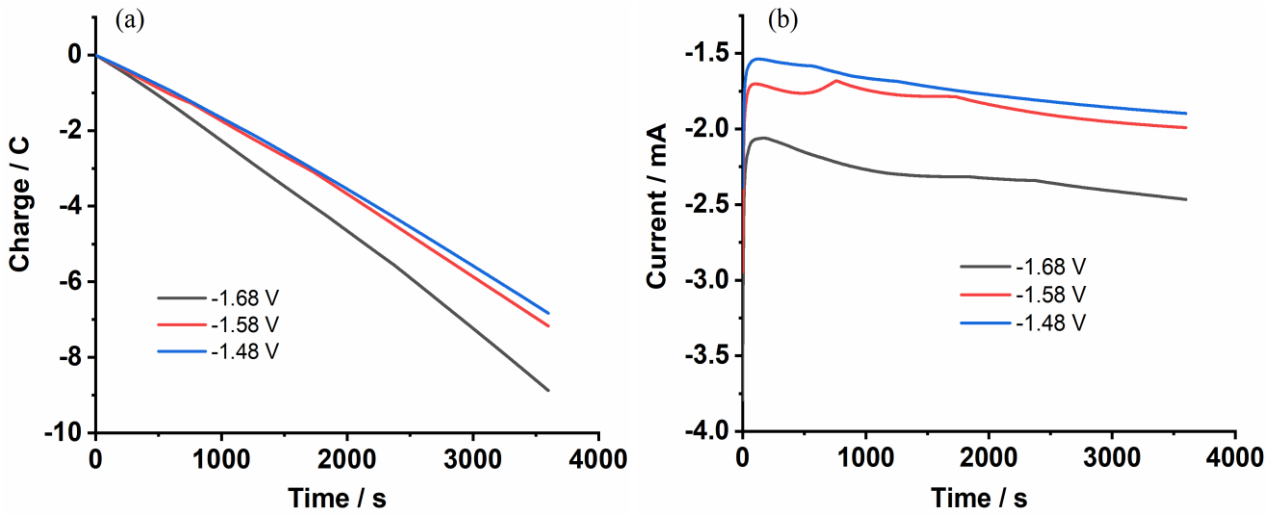

Fig. S17 (a) Charge-time curves and (b) current-time curves during the electrolysis of 0.5 mM Cudbes in 0.1 M $TBAPF_6$ CH_3CN solution in the presence of 88 equivalents of TFA at the potentials of -1.48 V, -1.58 V and -1.68 V. Glassy carbon working electrode.

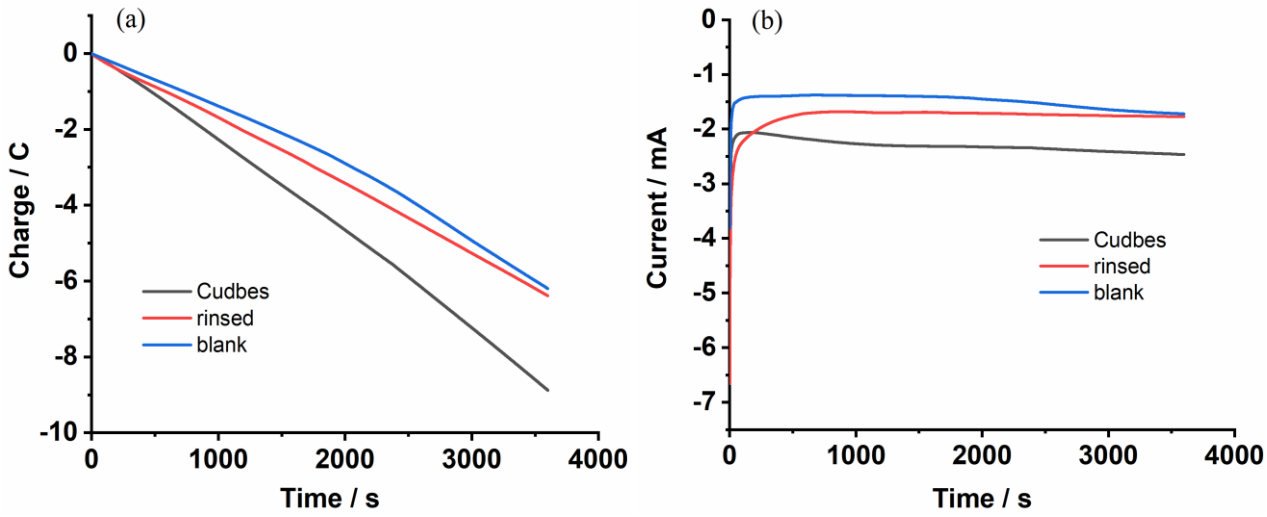

Fig. S18 (a) Charge-time curve and (b) current-time curve during the electrolysis of 0.5 mM Cudbes in 0.1 M $TBAPF_6$ CH_3CN solution in the presence of 88 equivalents of TFA at -1.68 V. Glassy carbon working electrode.

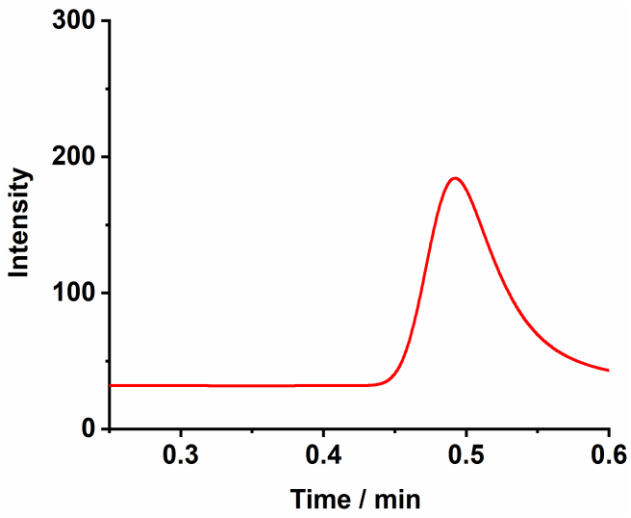

Fig. S19 Gas chromatographic spectrum of 0.5 mM Cudbes in 0.1 M $TBAPF_6$ CH_3CN containing 88 equivalents of TFA after the electrolysis at -1.68 V for 1 h.

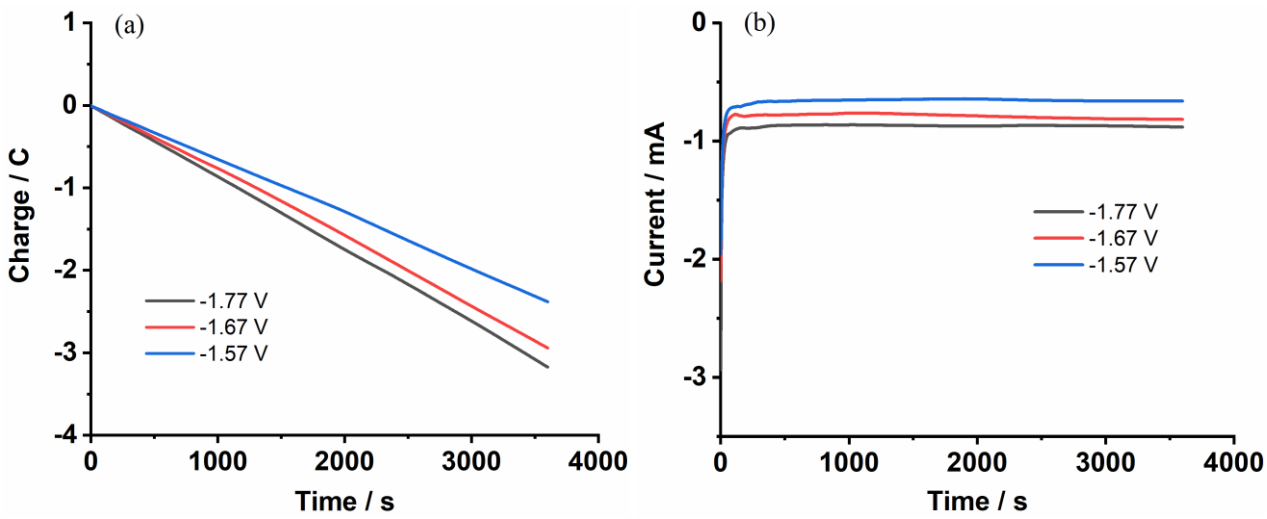

Fig. S20 (a) Charge-time curves and (b) current-time curves during the electrolysis of 0.5 mM Cudbes in 0.1 M $TBAPF_6$ CH_3CN solution in the presence of 72 equivalents of TsOH at the potentials of -1.57 V, -1.67 V and -1.77 V. Glassy carbon working electrode.

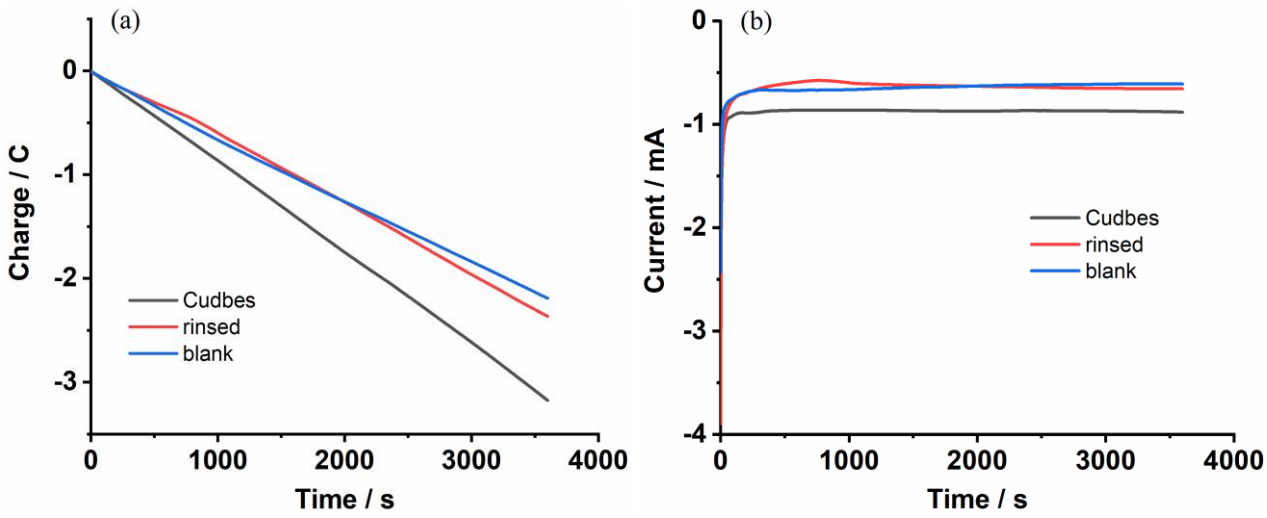

Fig. S21 (a) Charge-time curves and (b) current-time curves of the electrolysis of 0.5 mM Cudbes in 0.1 M $TBAPF_6$ CH_3CN solution in the presence of 72 equivalents of TsOH at the potential -1.77 V. Glassy carbon working electrode.

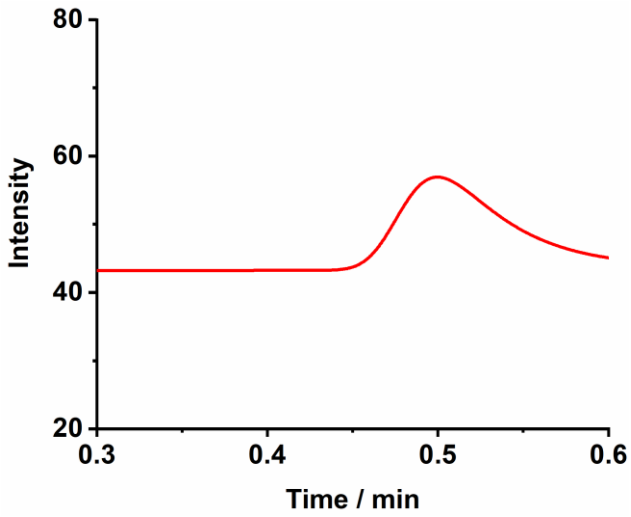

Fig. S22 Gas chromatographic spectrum of 0.5 mM Cudbes in 0.1 M $TBAPF_6$ CH_3CN containing 72 equivalents of TsOH after the electrolysis at -1.77 V for 1 h.

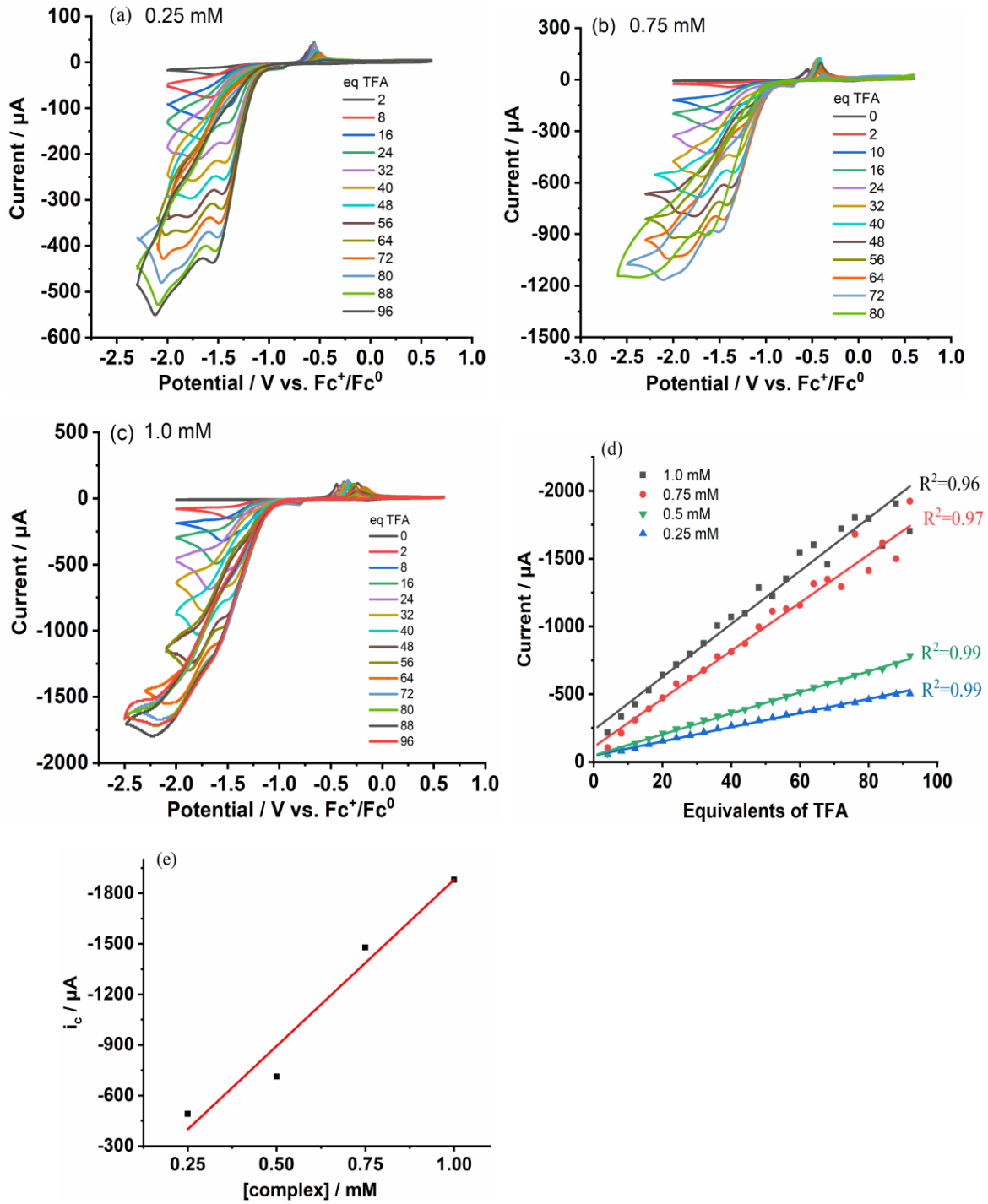

Fig. S23 Cyclic voltammograms in 0.1 M $TBAPF_6$ CH_3CN solutions in the presence of different concentrations of TFA for (a) 0.25 mM Cudbes, (b) 0.75 mM Cudbes, (c) 1.0 mM Cudbes. (d) Plots of the catalytic currents (i_c) vs the TFA concentration. (e) Plots of the catalytic current (i_c) vs the concentration of Cudbes in the presence of 88 equivalents of TFA. Glassy carbon working electrode, scan rate: 0.1 V s^{-1}.

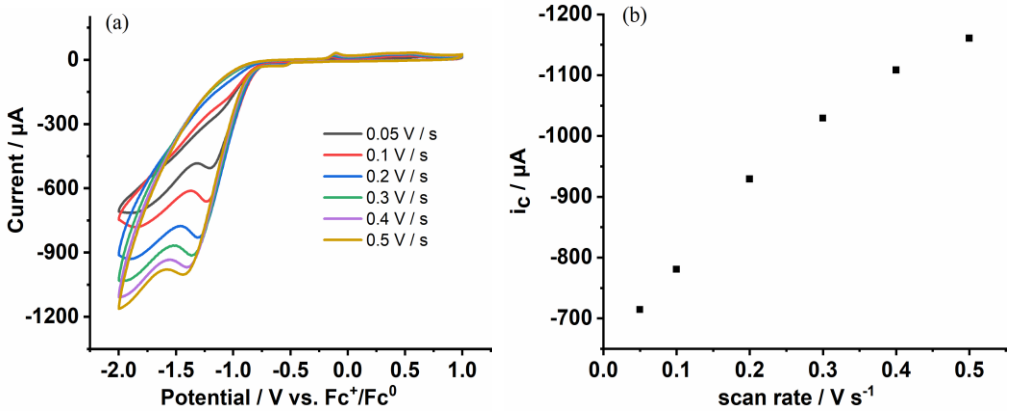

Fig. S24 (a) Cyclic voltammograms of 0.5 mM Cudbes in 0.1 M $TBAPF_6$ CH_3CN solution in the presence of 88 equivalents of TFA at scan rates of 0.05, 0.1, 0.2, 0.3, 0.4, and 0.5 V s^{-1}. (b) Plot of catalytic current (i_c) vs square root of scan rate. Glassy carbon working electrode.

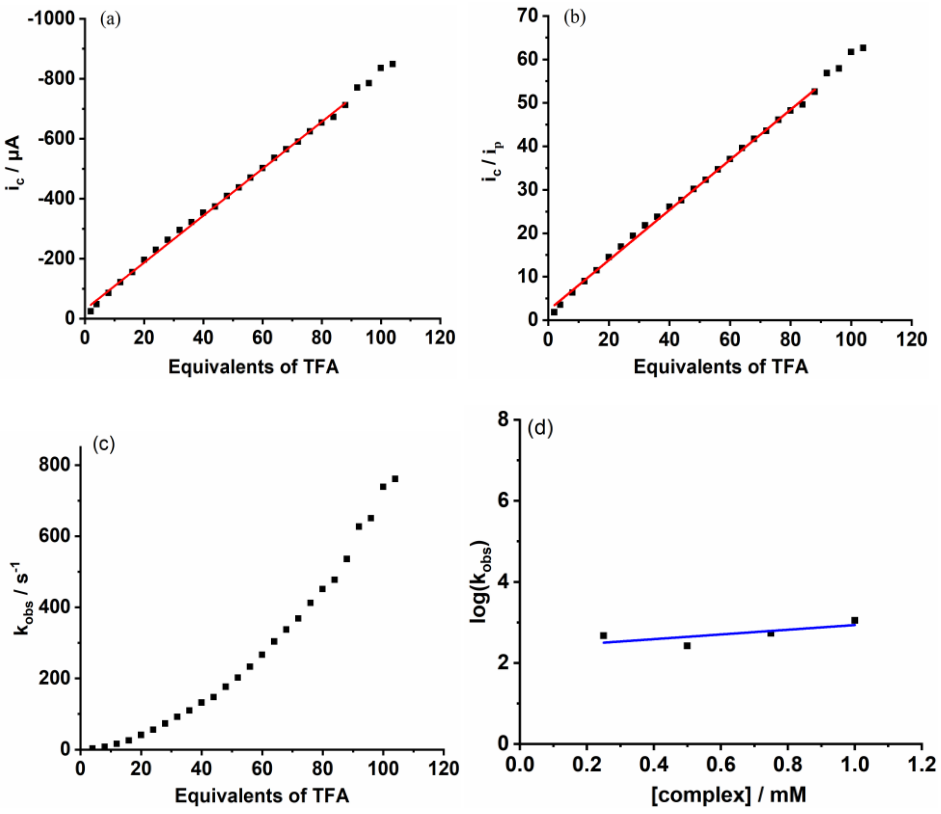

Fig. S25 (a) Plot of catalytic current (i_c) vs the concentration of TFA. (b) Plot of i_c/i_p vs the concentration of TFA. (c) Plot of k_{obs} vs the concentration of TFA. Conditions: 0.5 mM Cudbes in 0.1 M $TBAPF_6$ CH_3CN solution, glassy carbon working electrode, scan rate: 0.1 V s^{-1}. (d) Plot of k_{obs} vs the concentration of Cudbes in the presence of 88 equivalents of TFA. Concentration of Cudbes: 0.25 mM, 0.5 mM, 0.75 mM and 1.0 mM.

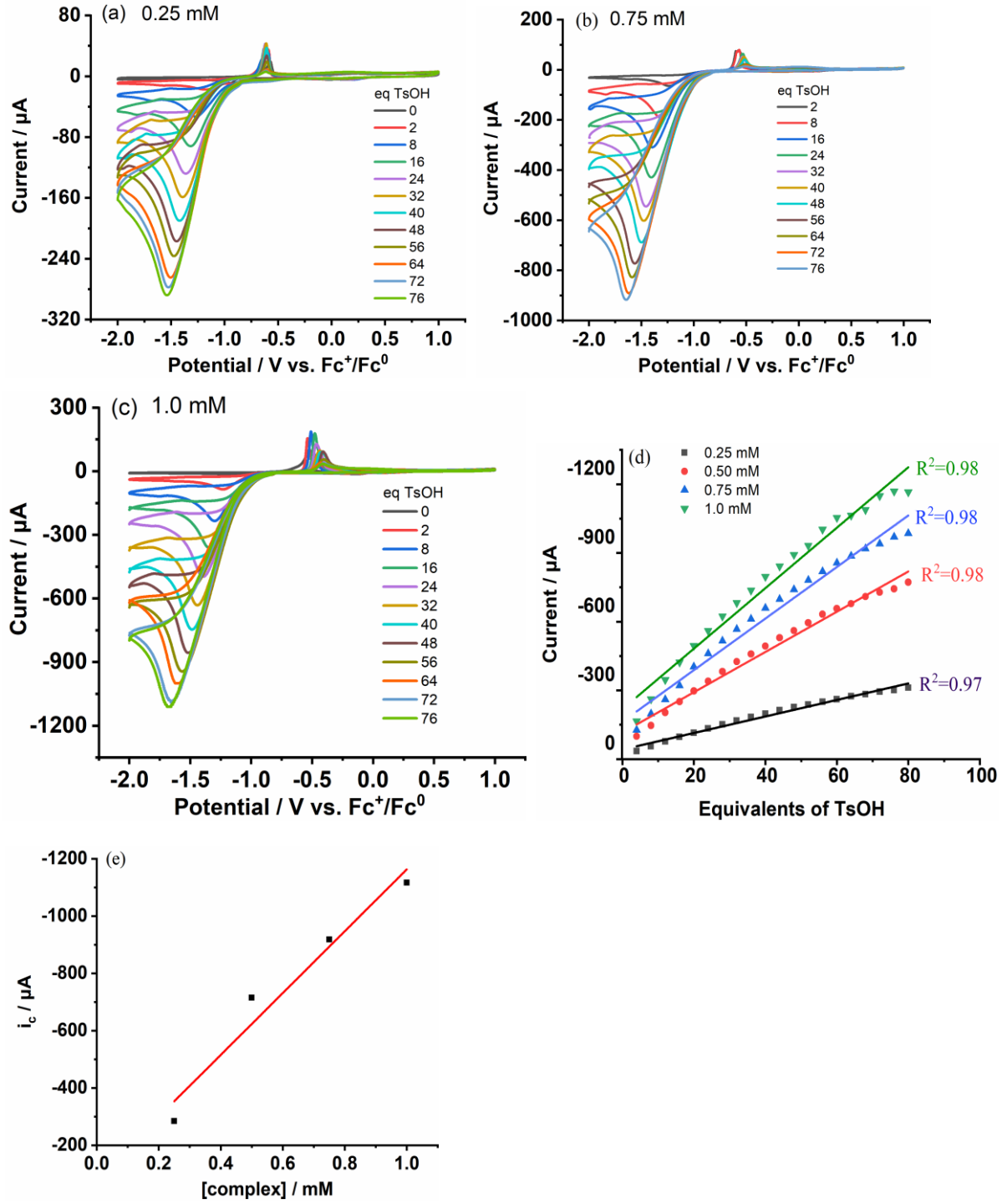

Fig. S26 Cyclic voltammograms in 0.1 M $TBAPF_6$ CH_3CN solutions in the presence of different concentrations of TsOH for (a) 0.25 mM Cudbes , (b) 0.75 mM Cudbes , (c) 1.0 mM Cudbes . (d) Plots of the catalytic currents (i_c) vs the concentration of TsOH. (e) Plots of the catalytic current (i_c) vs the concentration of Cudbes in the presence of 72 equivalents of TsOH. Glassy carbon working electrode, scan rate: 0.1 V s^{-1}.

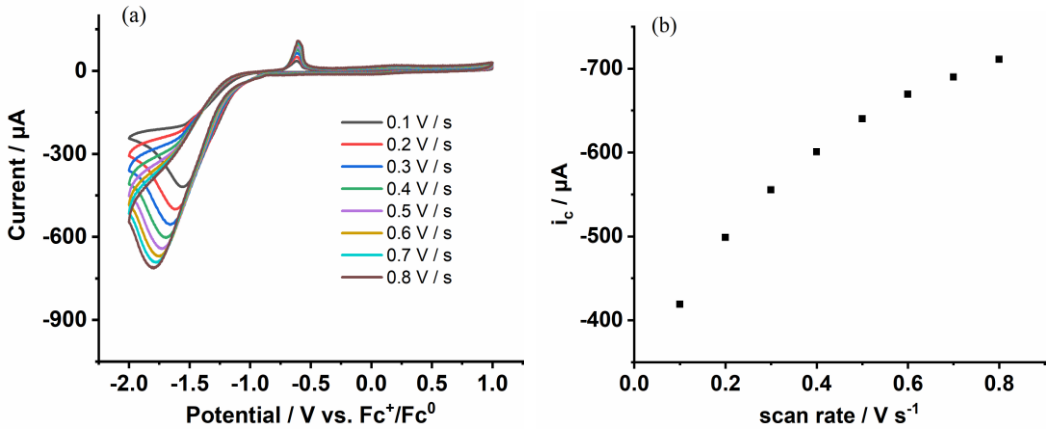

Fig. S27 (a) Cyclic voltammograms of 0.5 mM Cudbes in 0.1 M $TBAPF_6$ CH_3CN solution in the presence of 72 equivalents of TsOH at scan rates of 0.1, 0.2, 0.3, 0.4, 0.5, 0.6, 0.7 and 0.8 V s^{-1}. (b) Plot of catalytic current (i_c) vs square root of scan rate. Glassy carbon working electrode.

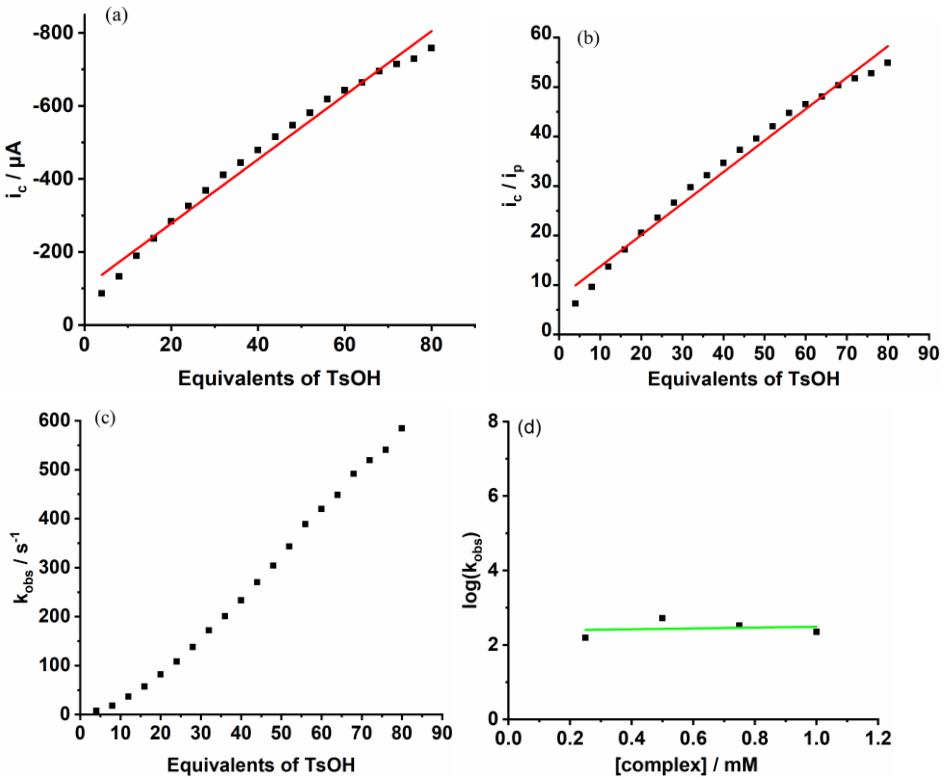

Fig. S28 (a) Plot of catalytic current (i_c) vs the concentration of TsOH. (b) Plot of i_c/i_p vs the concentration of TsOH. (c) Plot of k_{obs} vs the concentration of TsOH. Conditions: 0.5 mM Cudbes in 0.1 M $TBAPF_6$ CH_3CN solution, glassy carbon working electrode, scan rate: 0.1 V s^{-1}. (d) Plot of k_{obs} vs the concentration of Cudbes in the presence of 72 equivalents of TsOH. Concentration of Cudbes: 0.25 mM, 0.50 mM, 0.75 mM and 1.0 mM.

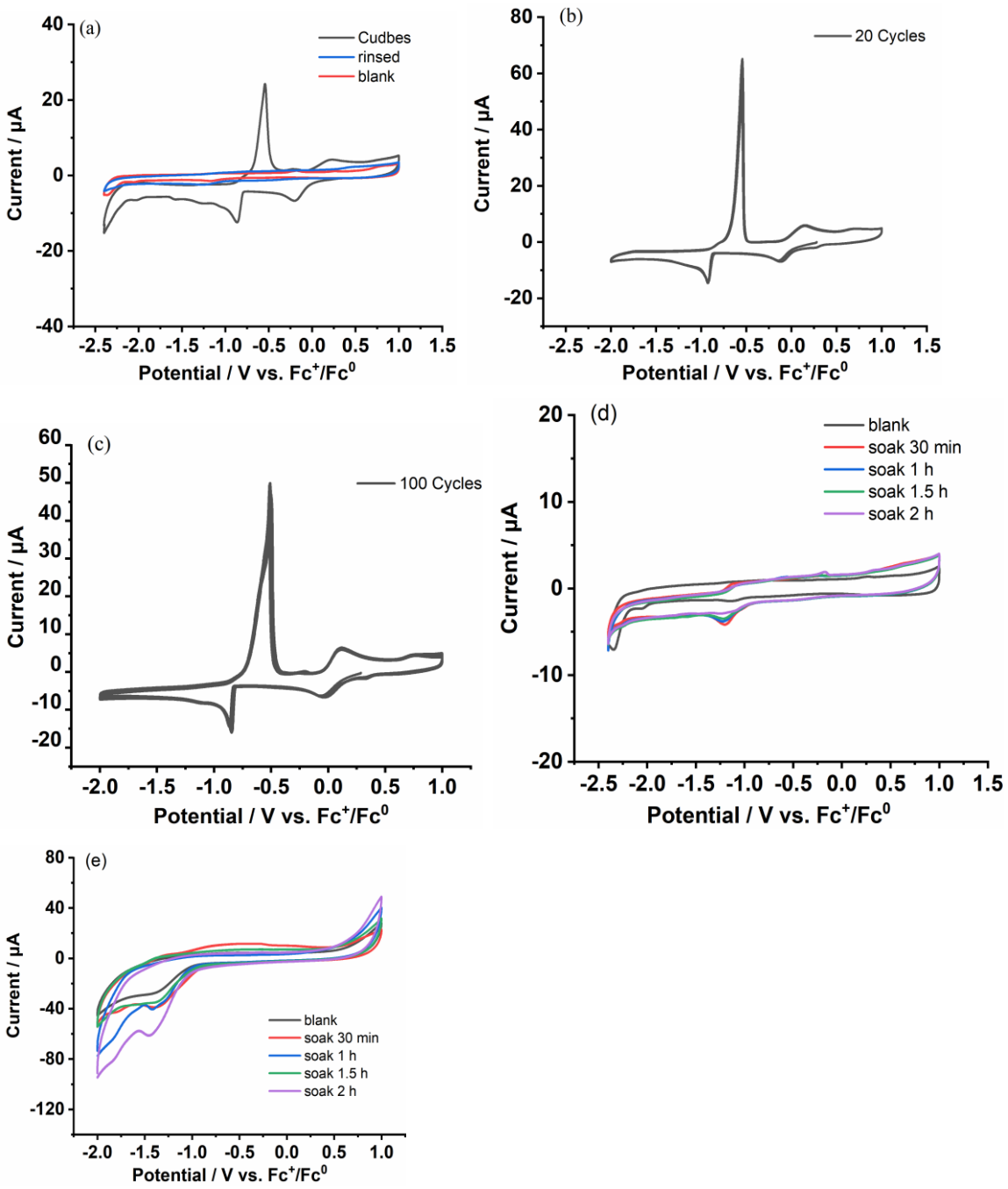

Fig. S29 Cyclic voltammograms using glassy carbon electrode in 0.1 M $TBAPF_6$ CH_3CN solution for (a) Cudbes, rinsed electrode and blank, (b) 20 consecutive cycles and (c) 100 consecutive cycles for Cudbes, (d) a glassy carbon electrode and (e) ITO electrodes obtained from the immersion into the solution of Cudbes for different times was using as working electrode in blank solution. Scan rate: 0.1 V s^{-1}. Concentration: 0.5 mM.

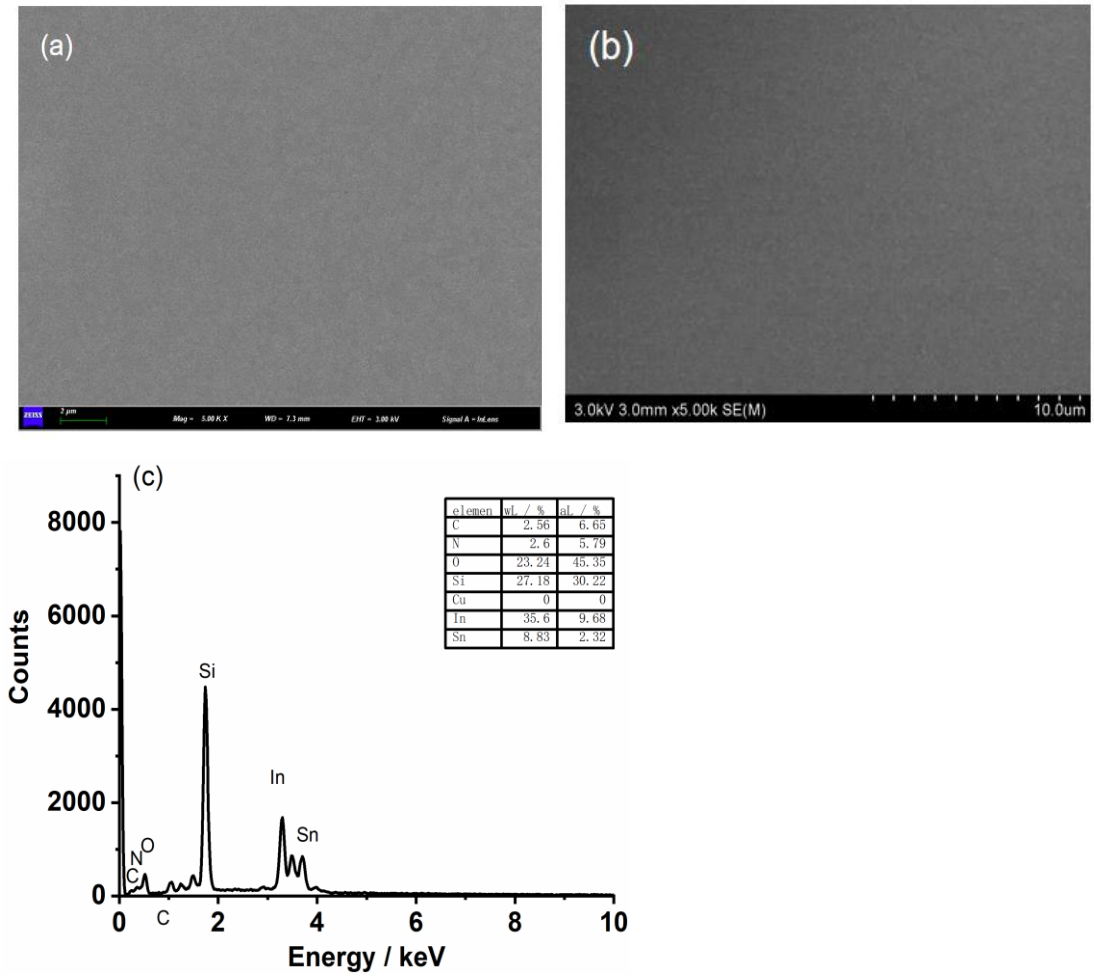

elemen	wt. / %	at. / %
C	2.56	6.65
N	2.6	5.79
O	23.24	45.35
Si	27.18	30.22
Cu	0	0
In	35.6	9.68
Sn	8.83	2.32

Fig. S30 (a) SEM image of a fresh ITO electrode. (b) SEM image and (c) EDS spectrum and data of an ITO electrode obtained from the immersion in a 0.5 mM Cudbes solution for 2 h.

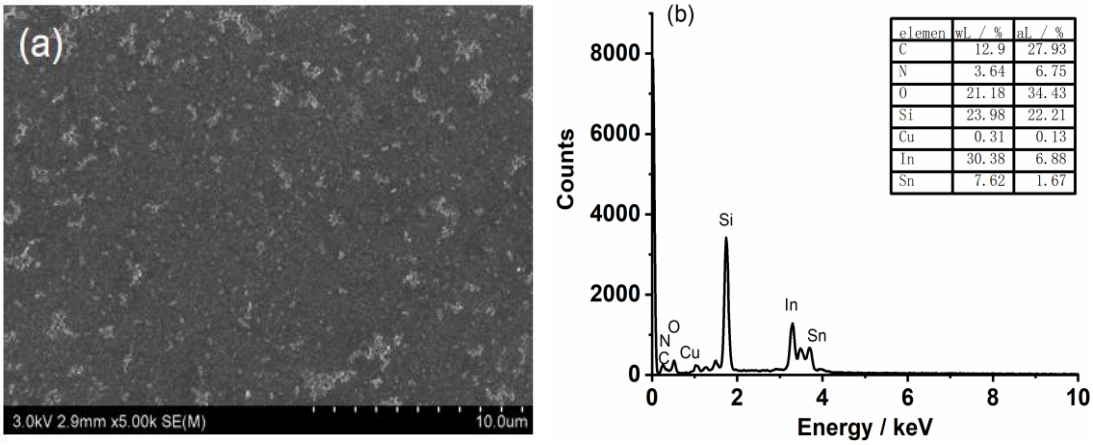

elemen	wt. / %	at. / %
C	12.9	27.93
N	3.64	6.75
O	21.18	34.43
Si	23.98	22.21
Cu	0.31	0.13
In	30.38	6.88
Sn	7.62	1.67

Fig. S31 (a) SEM image and (b) EDS spectrum and data of the ITO electrode obtained from consecutive 20 cycles in 0.5 mM Cudbes solution.

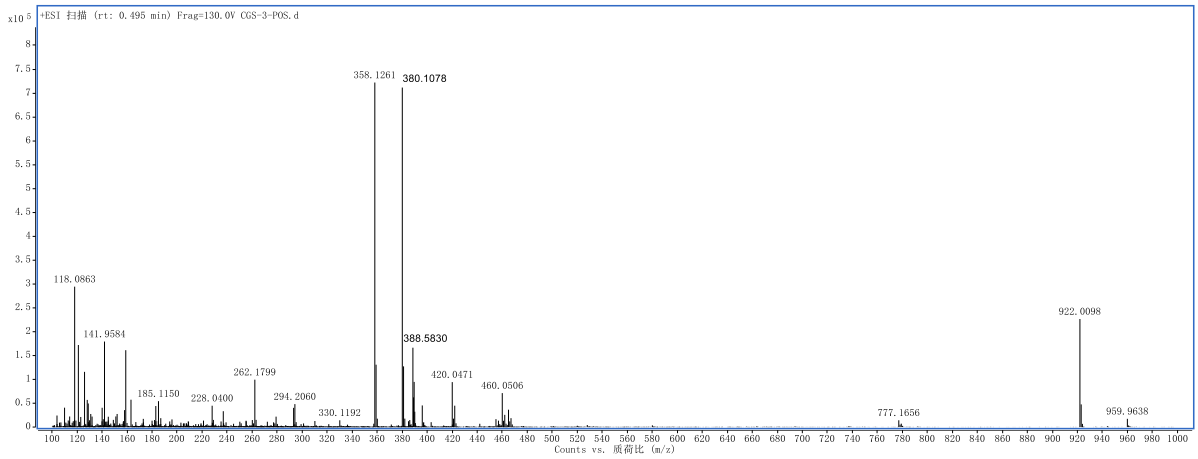

Fig. S32 Positive-ion electrospray ionization mass spectrum (ESI-MS) of Cudbes in CH_3CN in the presence of 30 equivalents of AcOH.

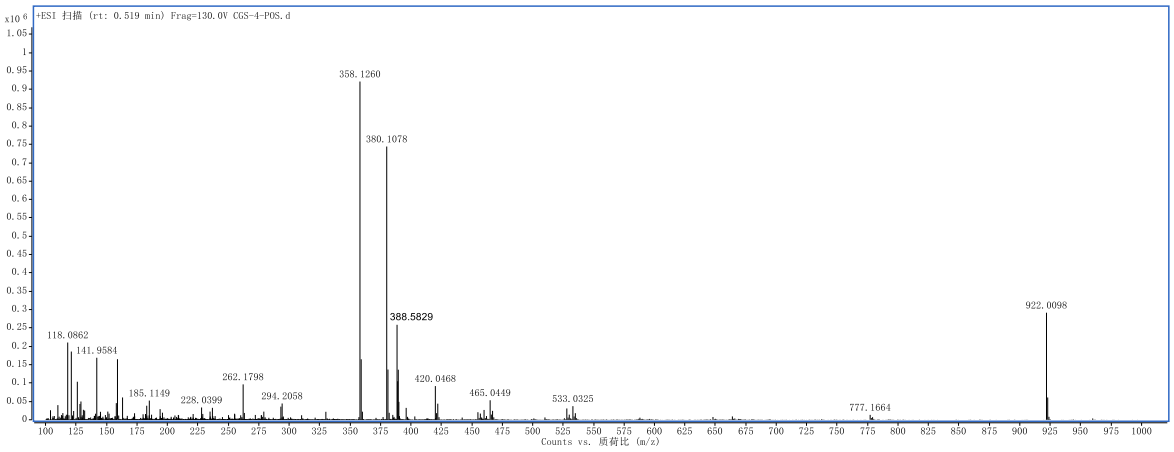

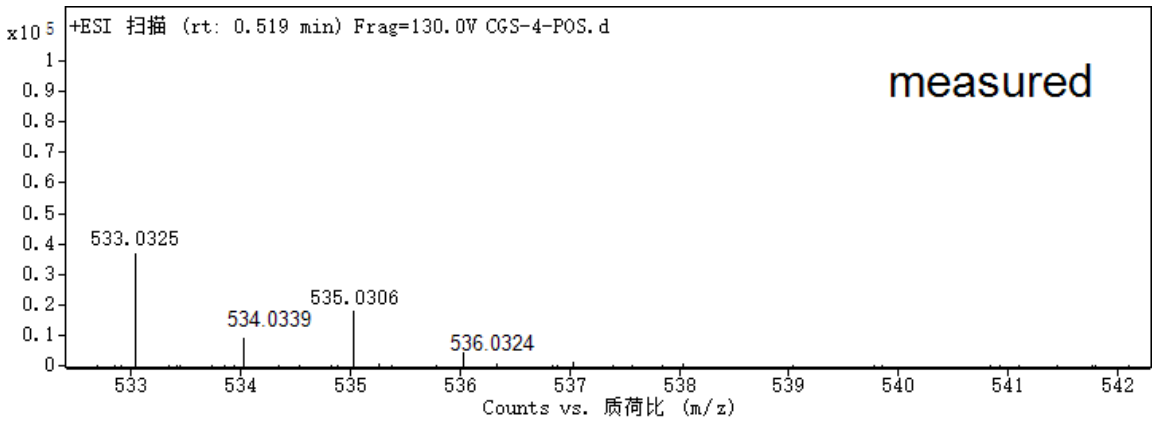

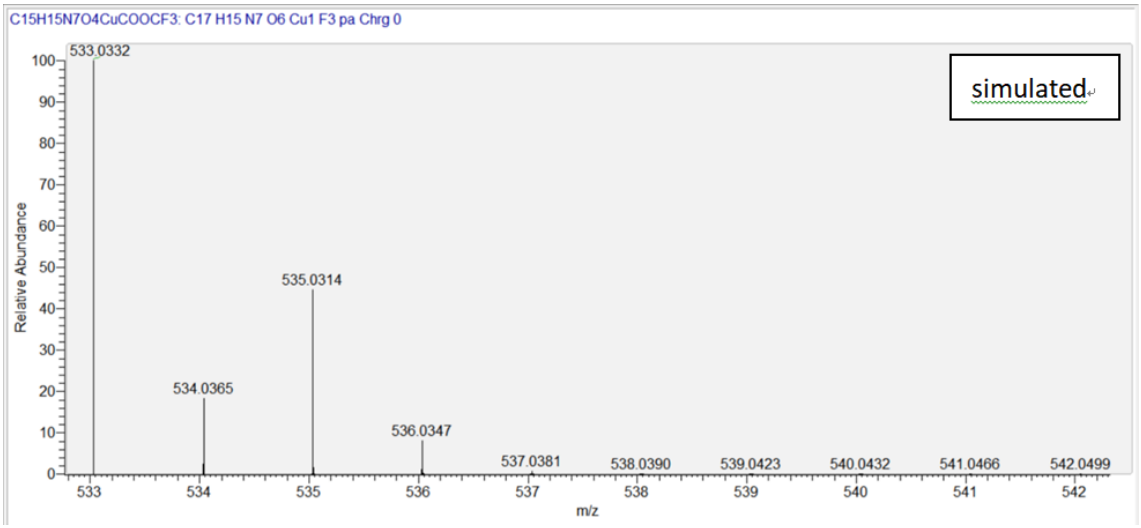

Fig. S33 Positive-ion electrospray ionization mass spectra (ESI-MS) of Cudbes in CH_3CN in the presence of 30 equivalents of TFA.

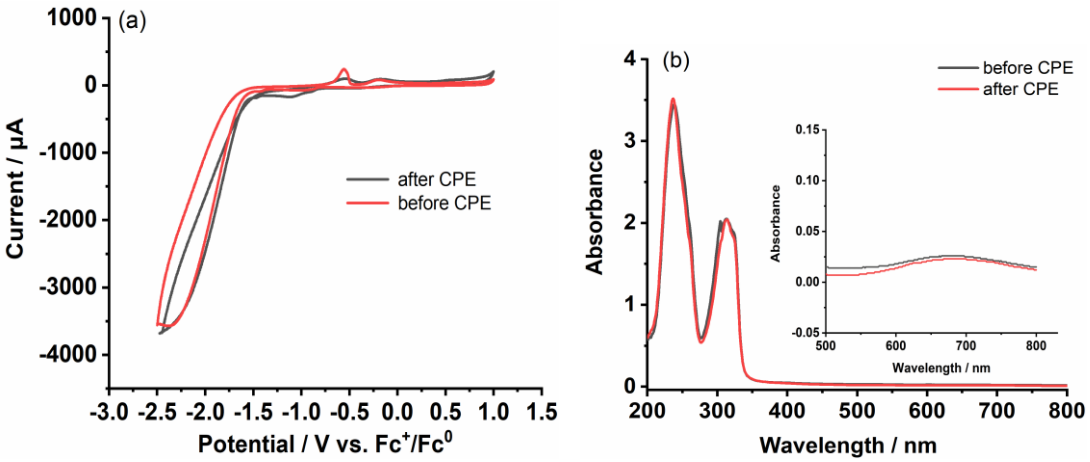

Fig. S34 (a) Cyclic voltammograms and (b) UV-vis absorption spectra of 0.5 mM Cudbes before and after the electrolysis at -1.90 V for 1 h. Conditions: in 0.1 M $TBAPF_6$ CH_3CN solution containing 200 equivalents of AcOH, glassy carbon working electrode, scan rate: 0.1 V s^{-1}.

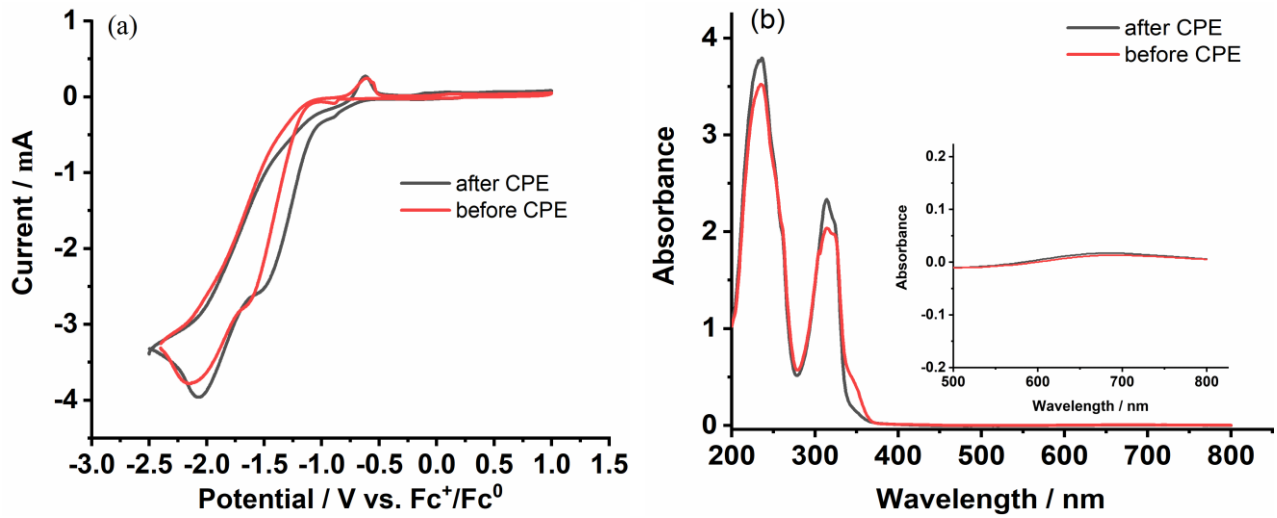

Fig. S35 (a) Cyclic voltammograms and (b) UV-vis absorption spectra of 0.5 mM Cudbes before and after the electrolysis at -1.68 V for 1 h. Conditions: in 0.1 M $TBAPF_6$ CH_3CN solution containing 88 equivalents of TFA, glassy carbon working electrode, scan rate: 0.1 V s^{-1}.

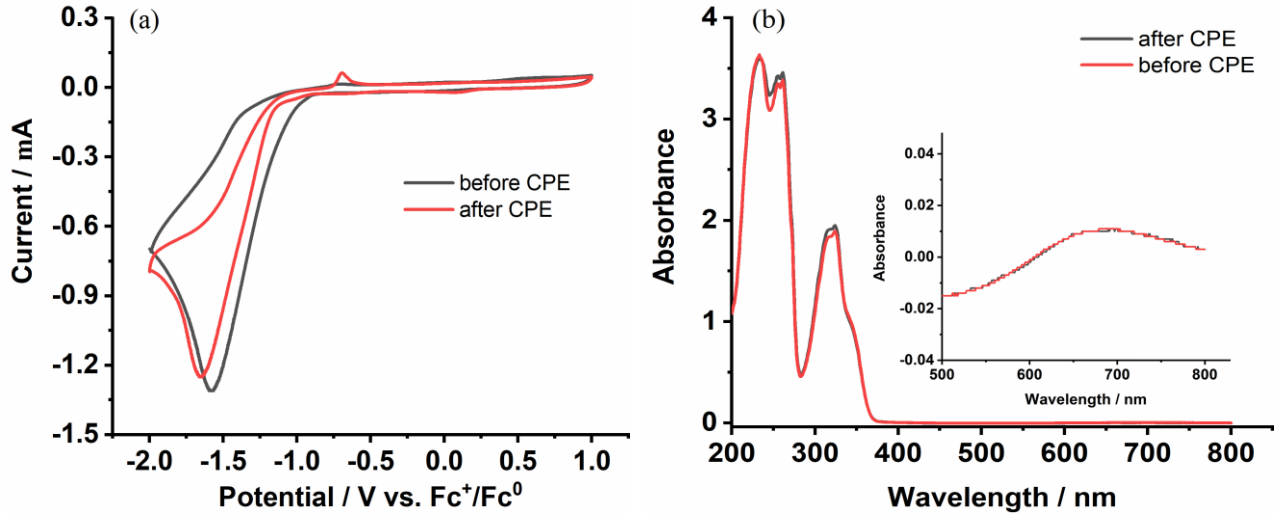

Fig. S36 (a) Cyclic voltammograms and (b) UV-Vis absorption spectra of 0.5 mM Cudbes before and after the electrolysis at -1.77 V for 1 h. Conditions: in 0.1 M $TBAPF_6$ CH_3CN solution containing 72 equivalents of TsOH, glassy carbon working electrode, scan rate: 0.1 V s^{-1}.

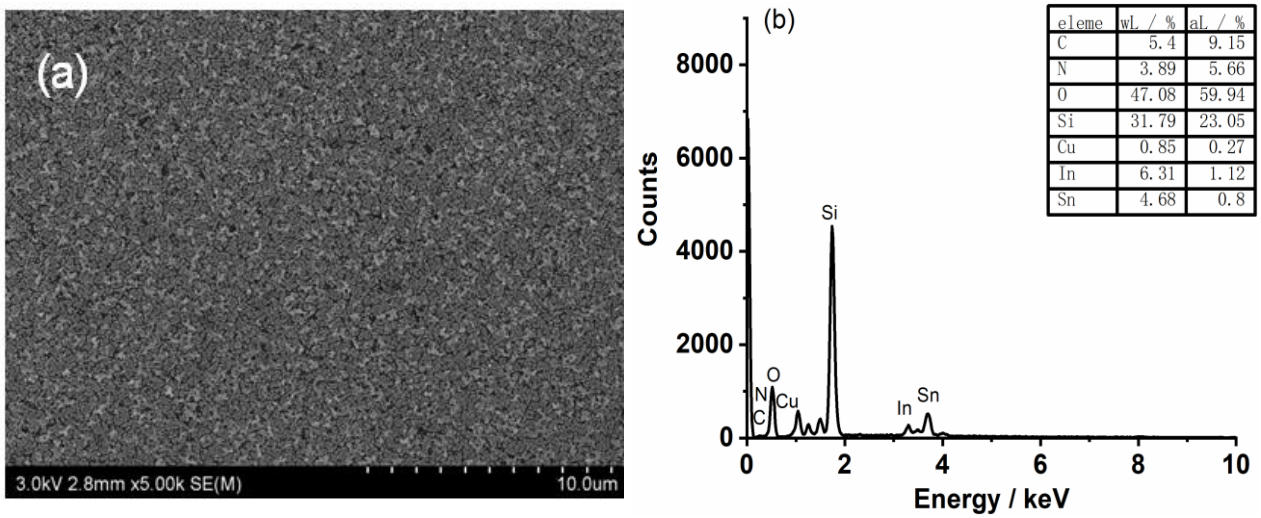

eleme	wL / %	aL / %
C	5.4	9.15
N	3.89	5.66
O	47.08	59.94
Si	31.79	23.05
Cu	0.85	0.27
In	6.31	1.12
Sn	4.68	0.8

Fig. S37 (a) SEM image and (b) EDS spectrum and data for an ITO electrode obtained from 20 consecutive cycles in 0.5 mM Cudbes CH_3CN solution with 200 equivalents of AcOH.

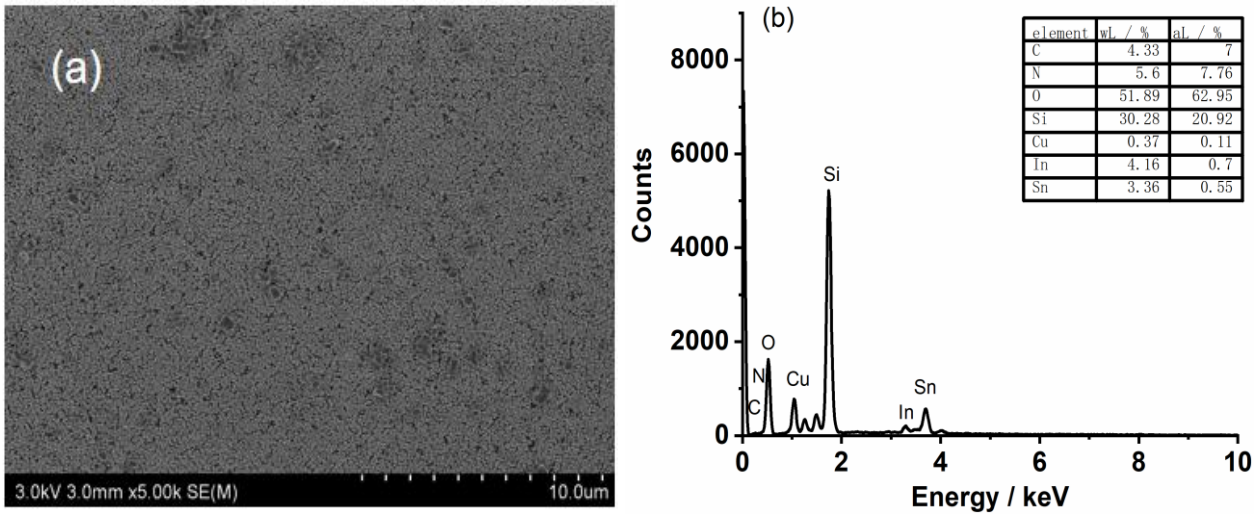

element	wL / %	aL / %
C	4.33	7
N	5.6	7.76
O	51.89	62.95
Si	30.28	20.92
Cu	0.37	0.11
In	4.16	0.7
Sn	3.36	0.55

Fig. S38 (a) SEM image and (b) EDS spectrum and data of the ITO electrode obtained from the electrolysis at -1.7 V for 1 h in 0.5 mM Cudbes CH_3CN solution with 200 equivalents of AcOH.

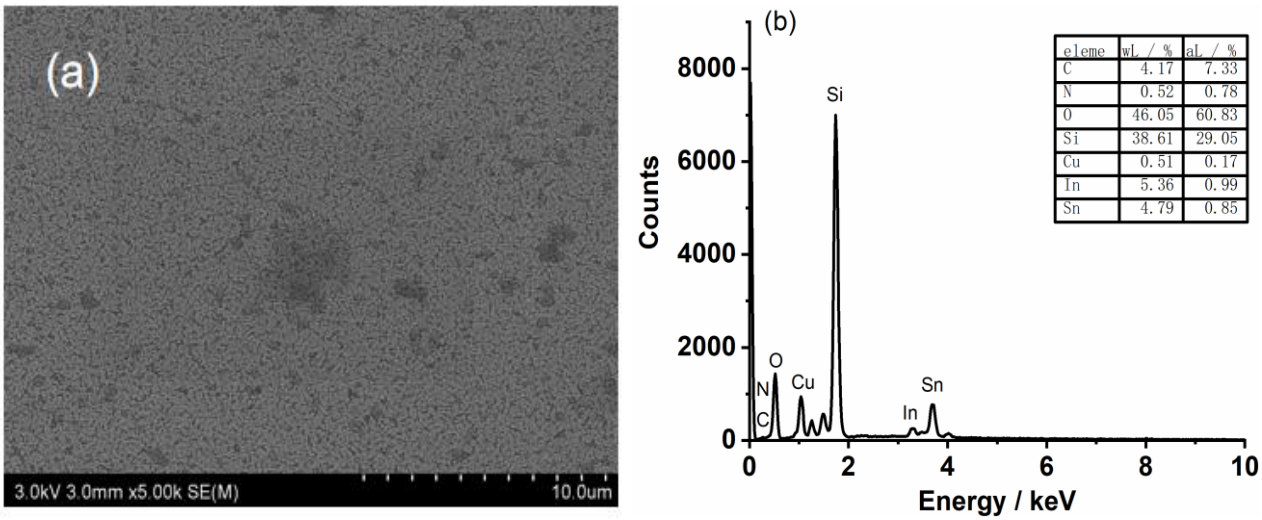

Fig. S39 (a) SEM image and (b) EDS spectrum and data for an ITO electrode obtained from 20 consecutive cycles in 0.5 mM Cudbes CH_3CN solution with 88 equivalents of TFA.

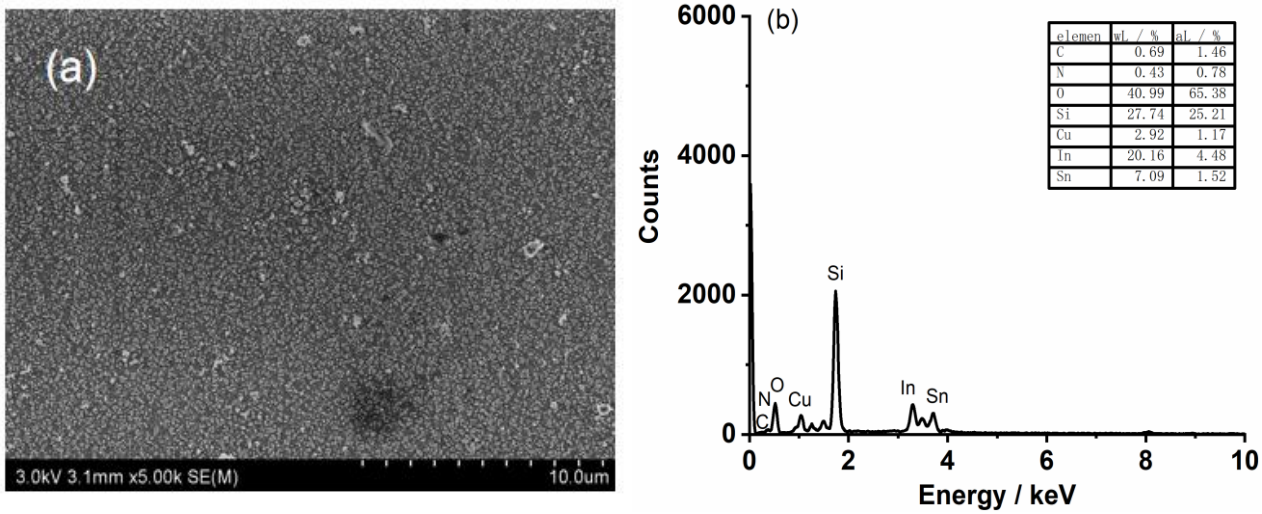

Fig. S40 (a) SEM image and (b) EDS spectrum and data of the ITO electrode obtained from the electrolysis at -1.7 V for 1 h in 0.5 mM Cudbes CH_3CN solution with 88 equivalents of TFA.

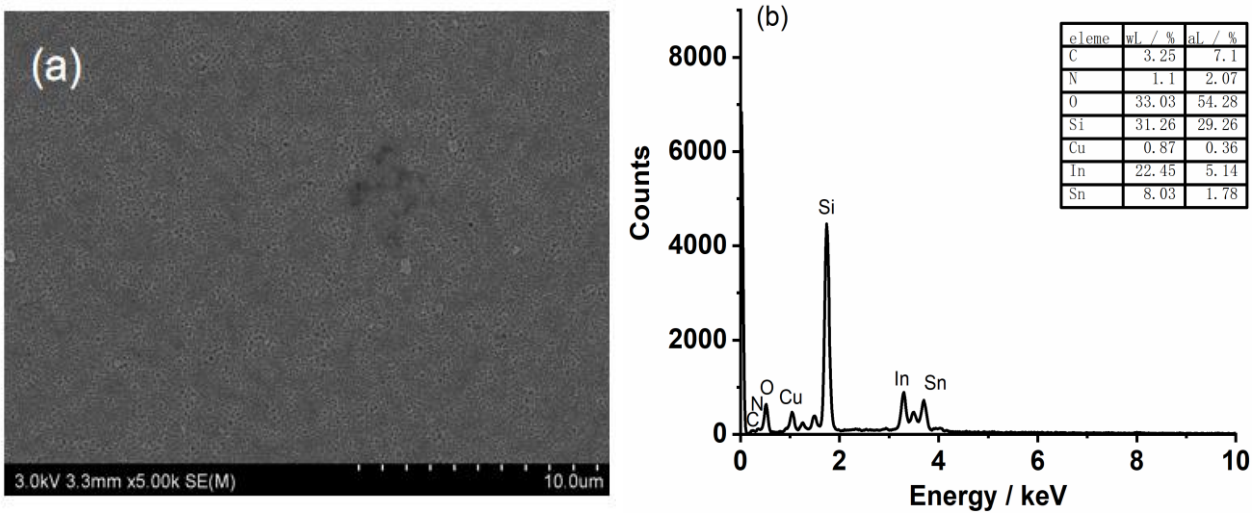

eleme	wL / %	aL / %
C	3.25	7.1
N	1.1	2.07
O	33.03	54.28
Si	31.26	29.26
Cu	0.87	0.36
In	22.45	5.14
Sn	8.03	1.78

Fig. S41 (a) SEM image and (b) EDS spectrum and data for an ITO electrode obtained from 20 consecutive cycles in 0.5 mM Cudbes CH_3CN solution with 72 equivalents of TsOH.

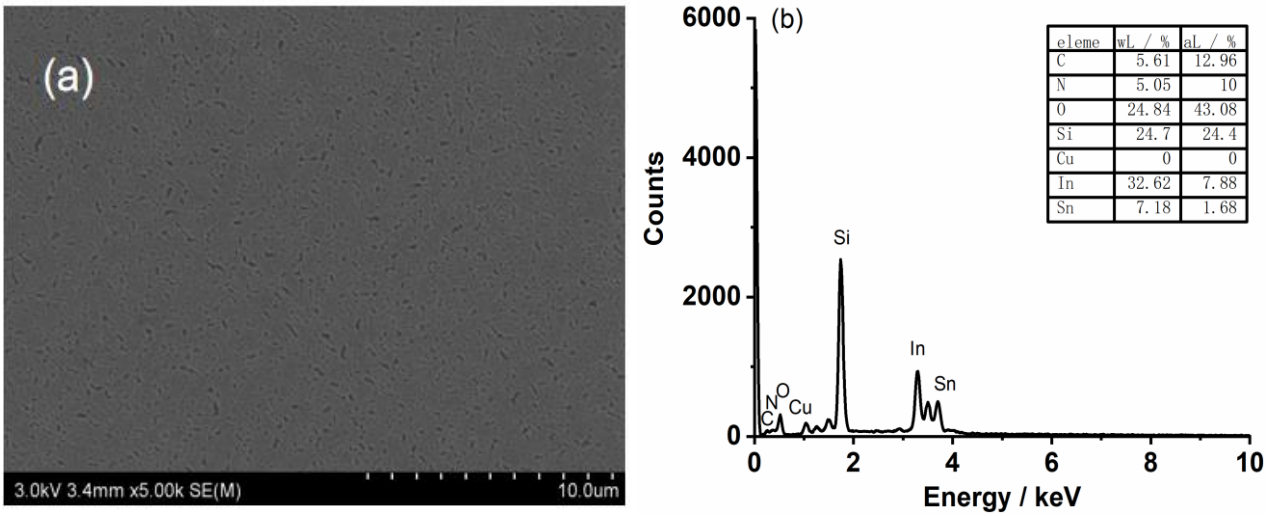

eleme	wL / %	aL / %
C	5.61	12.96
N	5.05	10
O	24.84	43.08
Si	24.7	24.4
Cu	0	0
In	32.62	7.88
Sn	7.18	1.68

Fig. S42 (a) SEM image and (b) EDS spectrum and data of the ITO electrode obtained from the electrolysis at -1.7 V for 1 h in 0.5 mM Cudbes CH_3CN solution with 72 equivalents of TsOH.

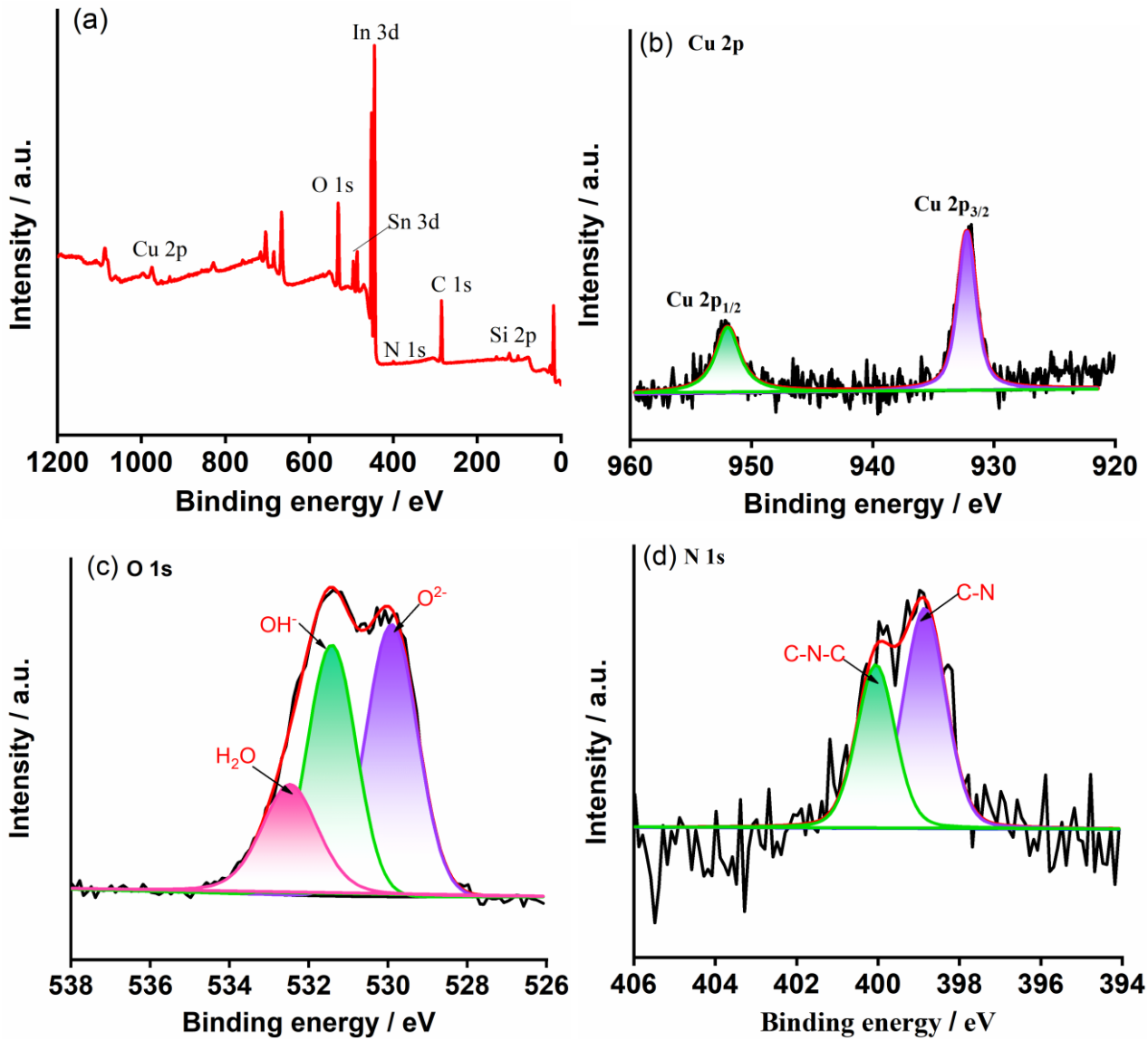

Fig. S43 (a) XPS survey data of the ITO electrode obtained from the electrolysis at -1.7 V for 1 h in 0.5 mM Cudbes CH_3CN solution with 200 equivalents of AcOH, (b) high-resolution XPS spectrum of Cu 2p region, (c) high-resolution XPS spectrum of O 1s region, (d) high-resolution XPS spectrum of N 1s region.

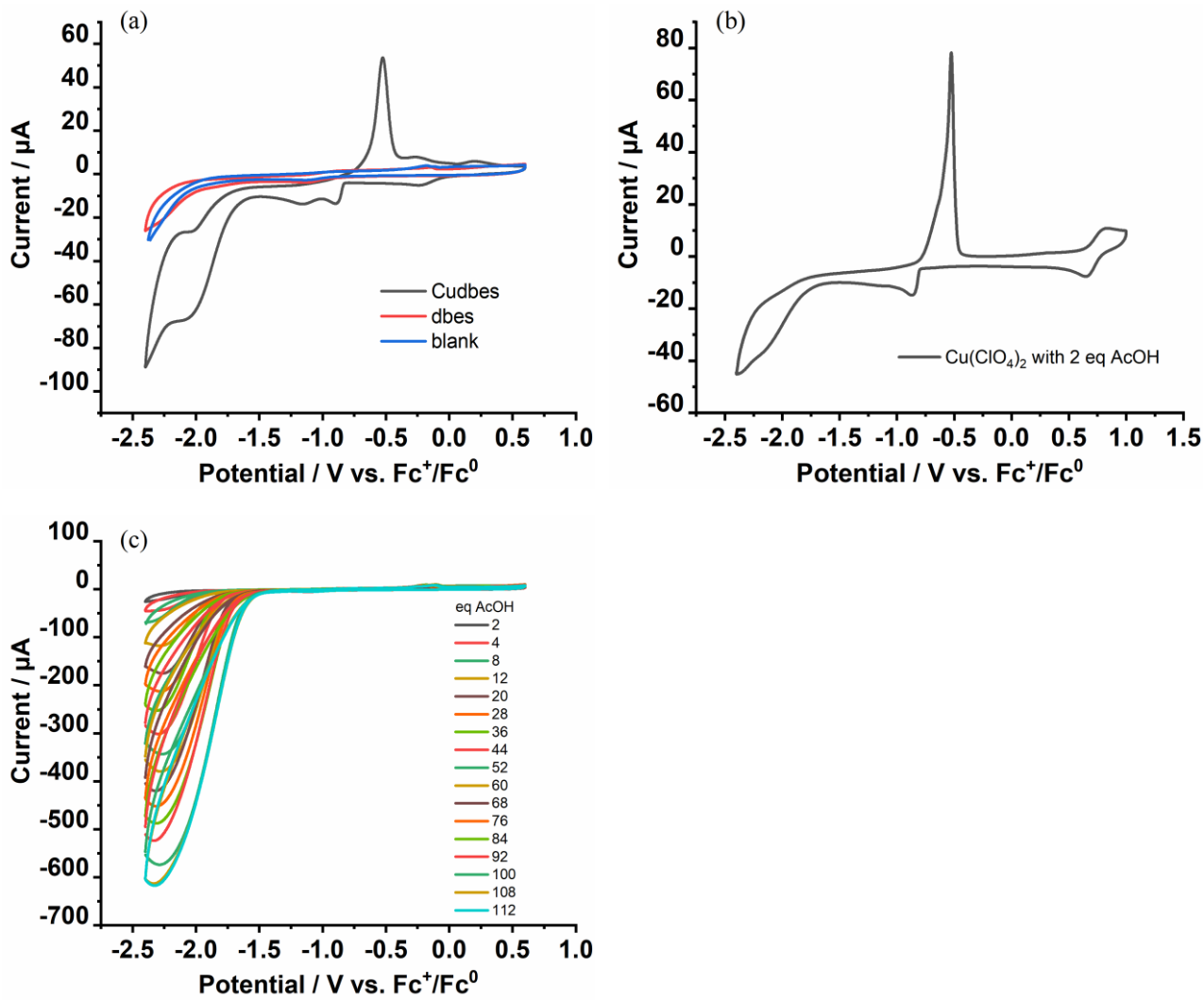

Fig. S44 (a) Cyclic voltammograms of Cudbes, dbes and blank solution in the presence of 2 equivalents of AcOH. (b) $Cu(ClO_4)_2$ with 2 equivalents of AcOH. (c) dbes with different concentrations of AcOH. Conditions: in 0.1 M $TBAPF_6$ CH_3CN solution, glassy carbon working electrode, scan rate: 0.1 V s^{-1}. Sample concentration: 0.5 mM.

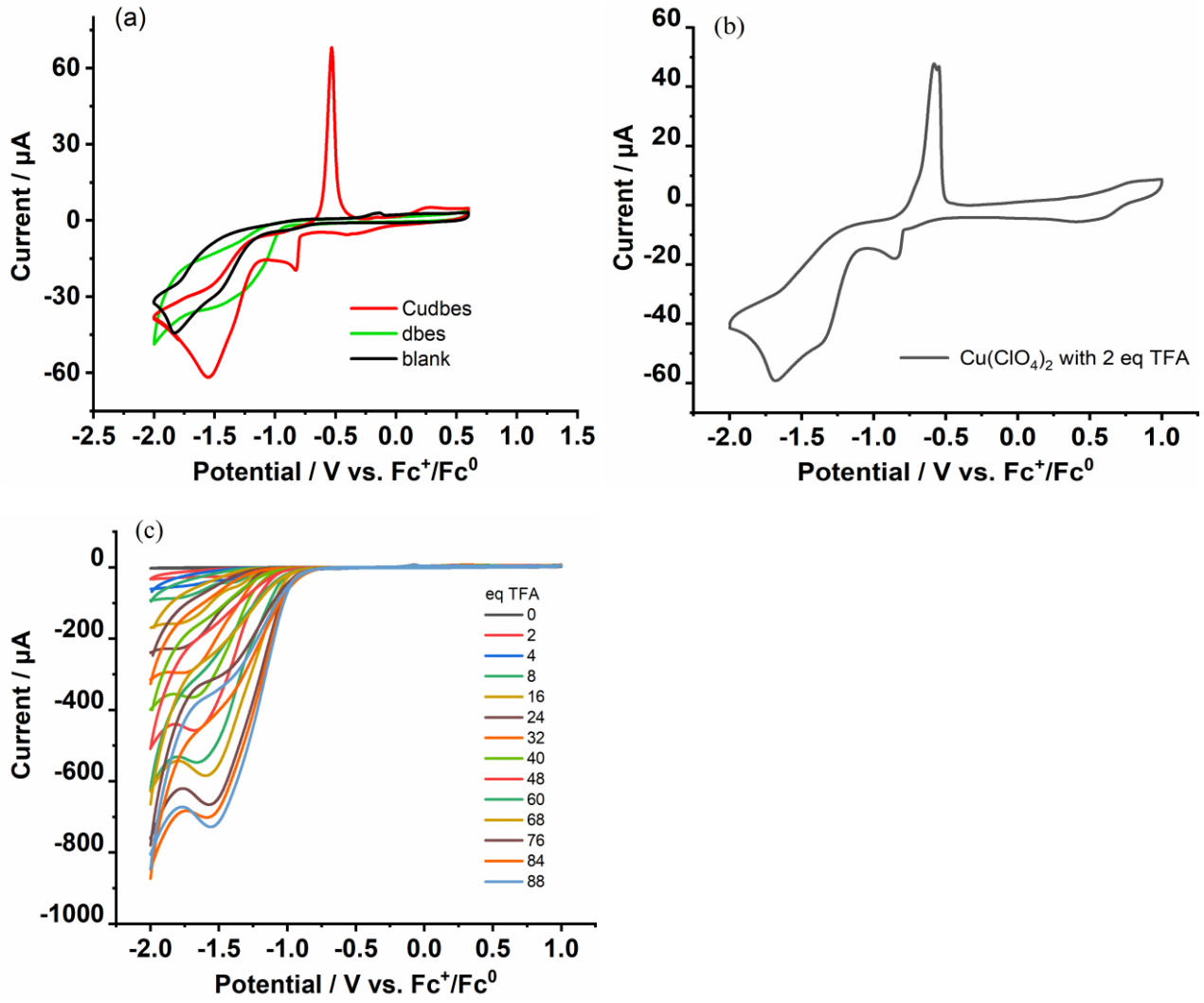

Fig. S45 (a) Cyclic voltammograms of Cudbes, dbes and blank solution in the presence of 2 equivalents of TFA. (b) $Cu(ClO_4)_2$ with 2 equivalents of TFA. (c) dbes with different concentrations of TFA. Conditions: in 0.1 M $TBAPF_6$ CH_3CN solution, glassy carbon working electrode, scan rate: 0.1 V s^{-1}. Sample concentration: 0.5 mM.

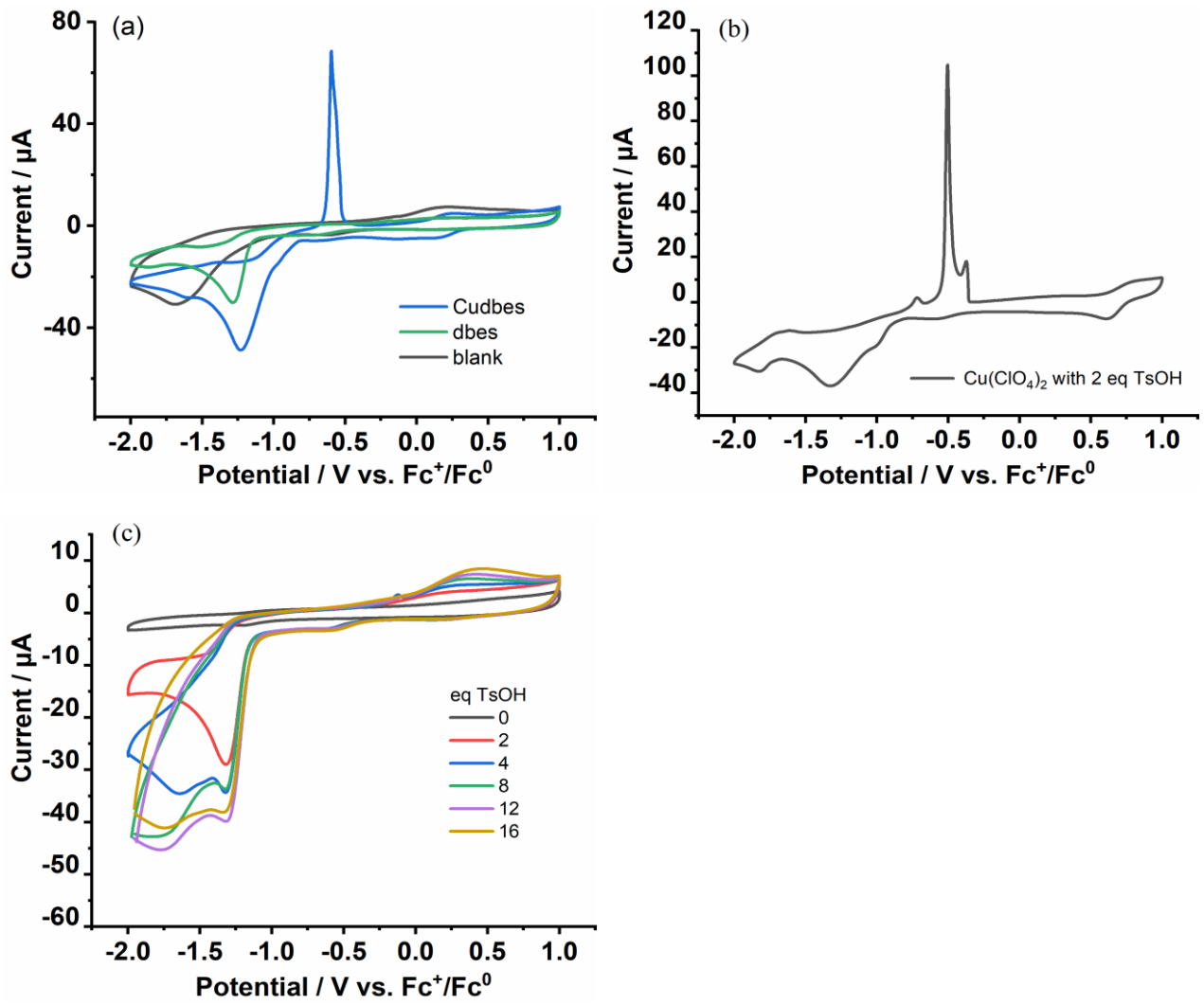

Fig. S46 (a) Cyclic voltammograms of Cudbes, dbes and blank solution in the presence of 2 equivalents of TsOH. (b) $Cu(ClO_4)_2$ with 2 equivalents of TsOH. (c) dbes with different concentrations of TsOH. Conditions: in 0.1 M $TBAPF_6$ CH_3CN solution, glassy carbon working electrode, scan rate: 0.1 V s^{-1}. Sample concentration: 0.5 mM.

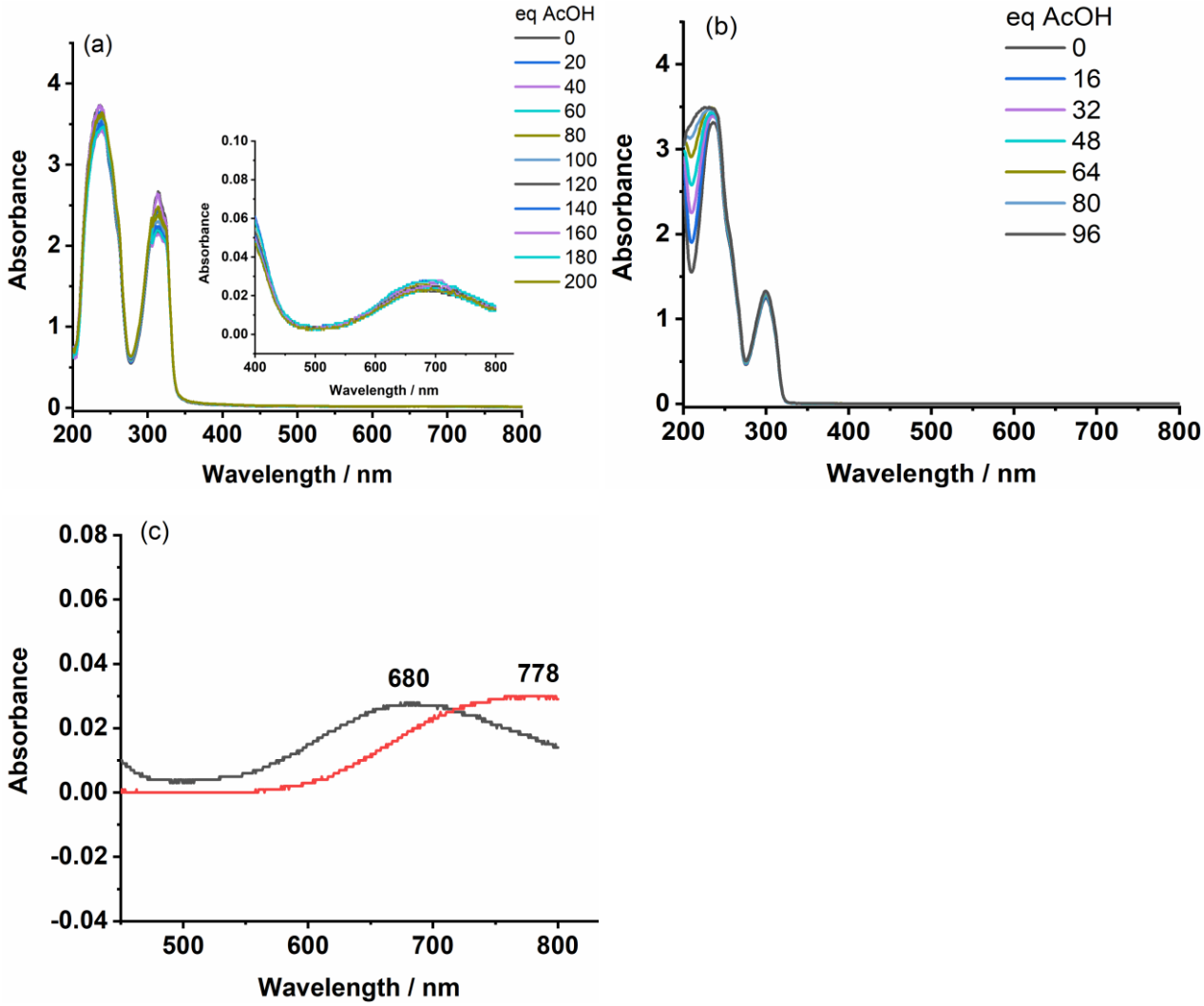

Fig. S47 UV-vis absorption spectra of (a) Cudbes in CH_3CN in the presence of AcOH (0-200 equivalents), (b) dbes in CH_3CN with AcOH (0-96 equivalents), (c) $Cu(ClO_4)_2$ (red line) and Cudbes (black line) in CH_3CN with 200 equivalents of AcOH. Sample concentration: 0.1 mM.

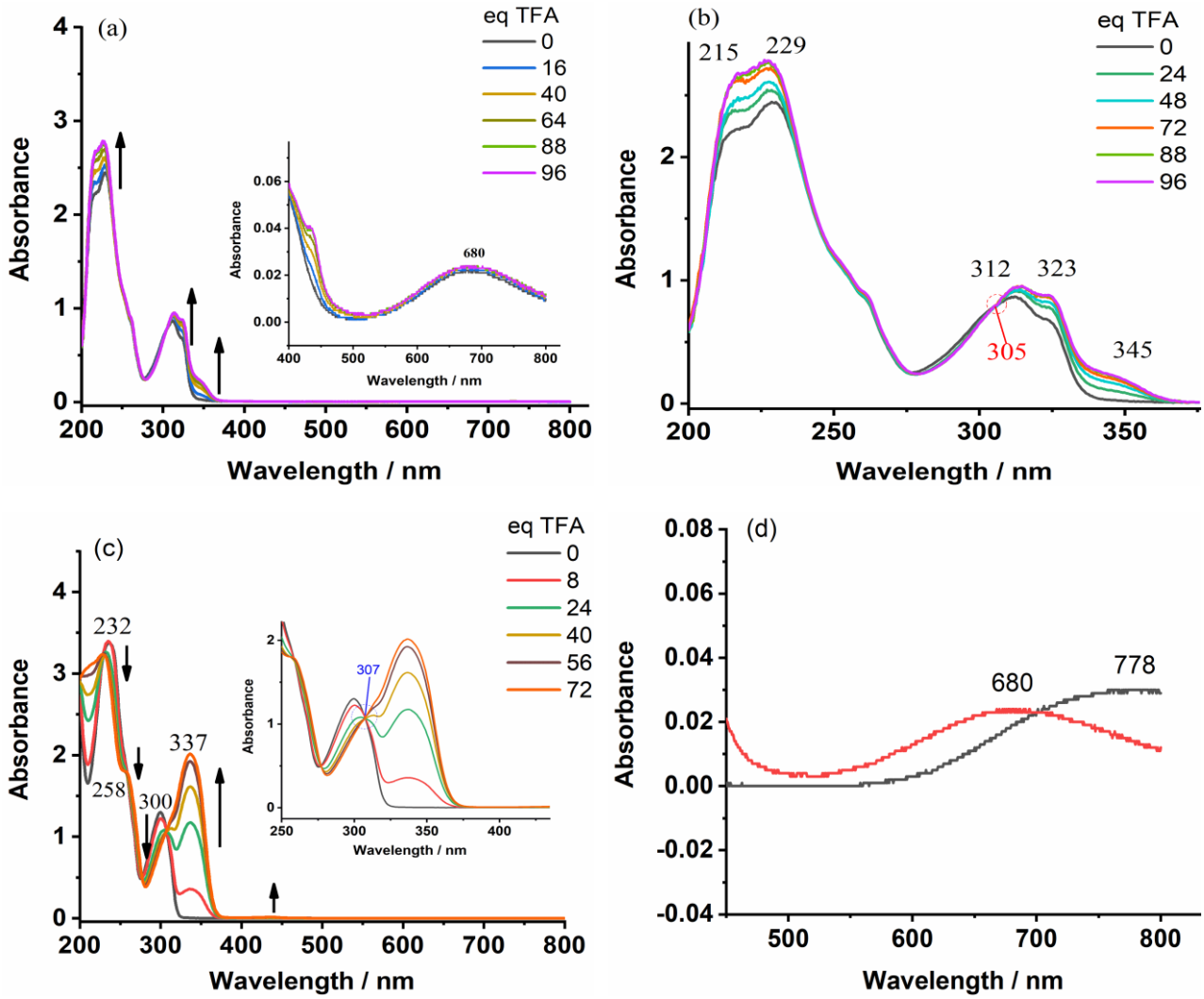

Fig. S48 (a) UV-vis absorption spectra of Cudbes in CH_3CN with TFA (0-96 equivalents), (b) Enlarged view of Fig. (a). (c) UV-vis absorption spectra of dbes in CH_3CN with TFA (0-72 equivalents). (d) UV-vis absorption spectra of $Cu(ClO_4)_2$ (black line) and Cudbes (red line) in CH_3CN with 88 equivalents of TFA. Sample concentration: 0.1 mM.

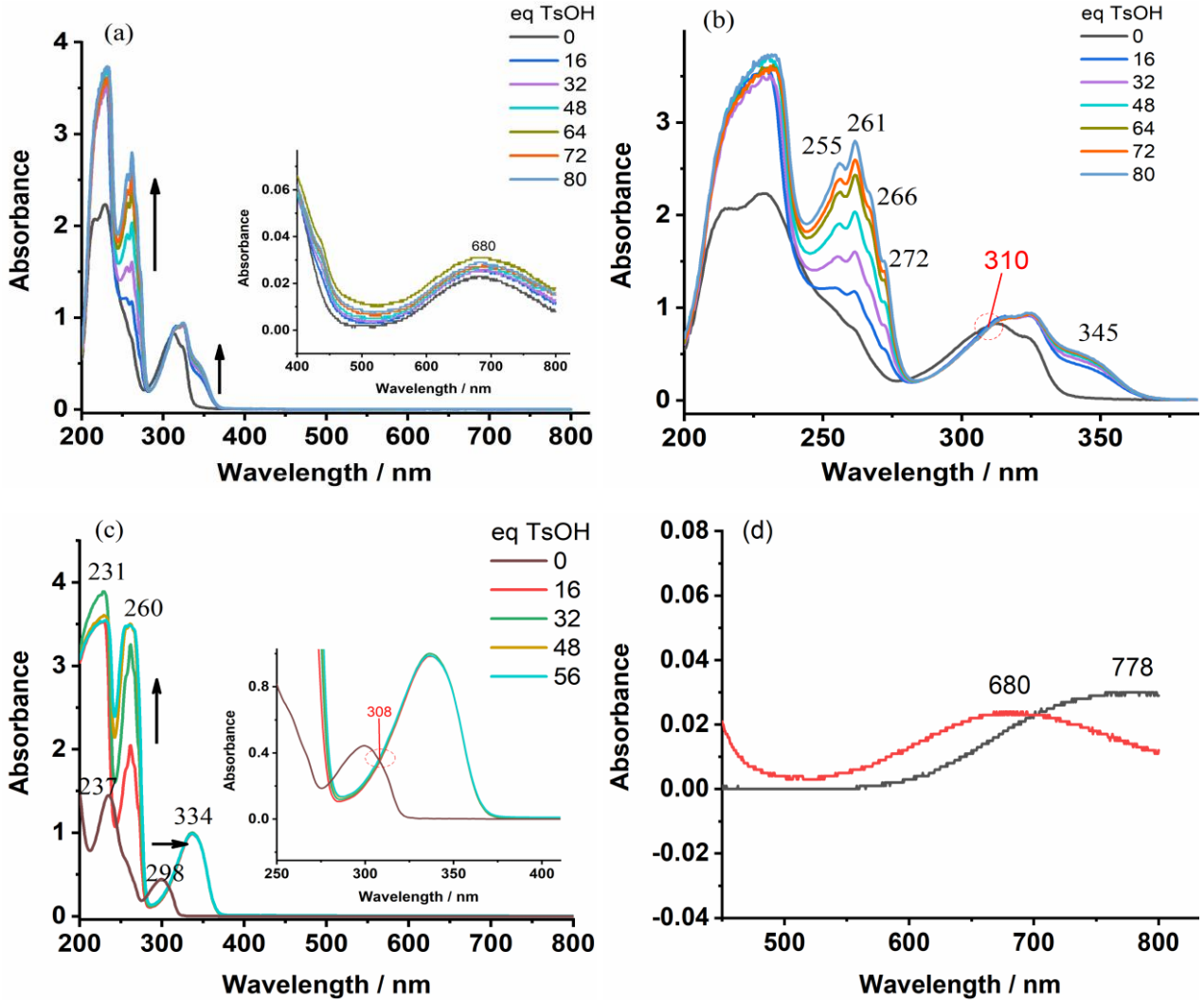

Fig. S49 (a) UV-vis absorption spectra of Cudbes in CH_3CN with TsOH (0-80 equivalents). (b) Enlarged view of Fig. (a). (c) UV-vis absorption spectra of dbes in CH_3CN with TsOH (0-56 equivalents). (d) UV-vis absorption spectra of $Cu(ClO_4)_2$ (black line) and Cudbes (red line) in CH_3CN with 72 equivalents of TsOH. Sample concentration: 0.1 mM.

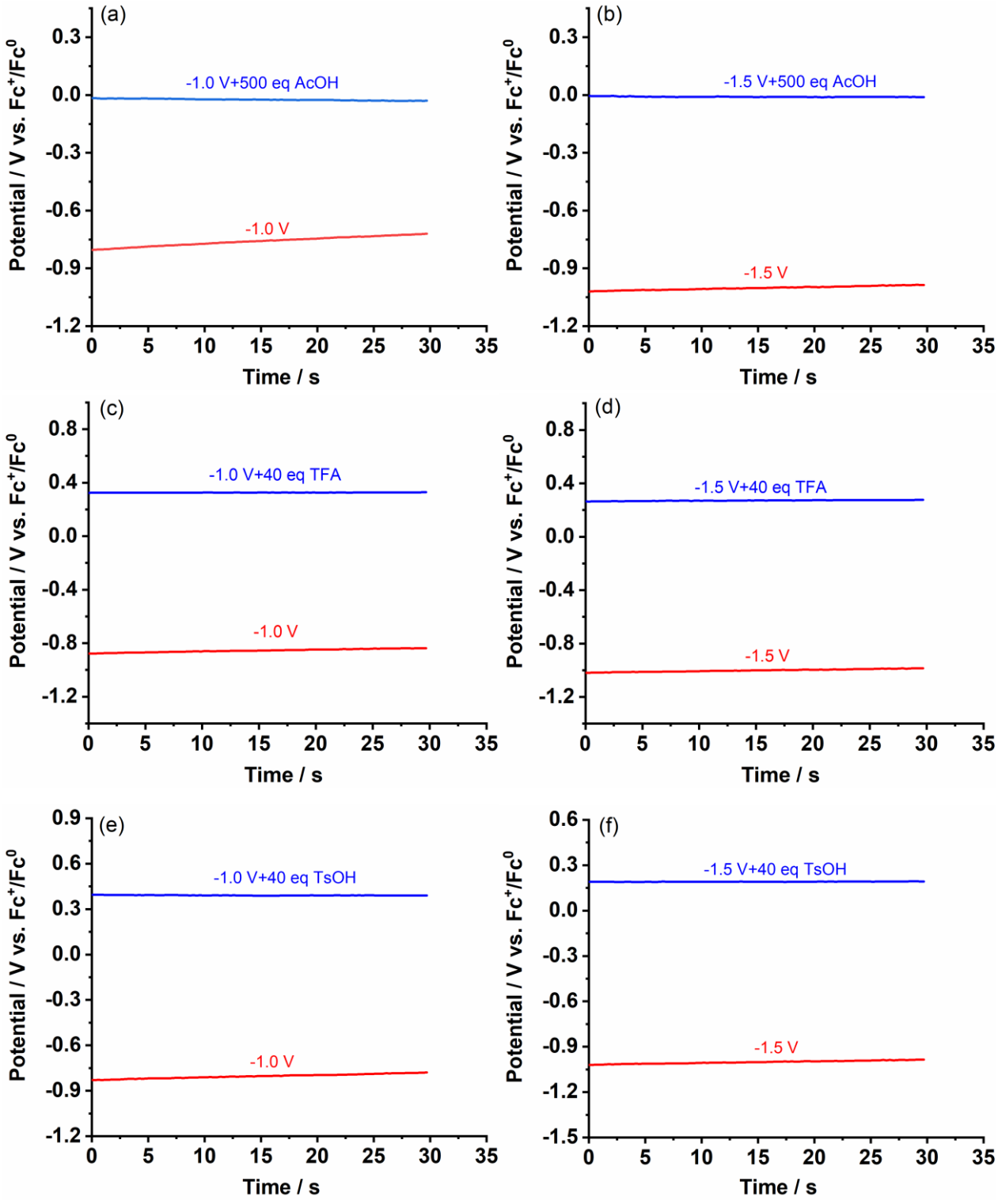

Fig. S50 Plots of time-dependent open circuit potential (OCP) of 0.5 mM Cudbes in 0.1 M $TBAPF_6$ CH_3CN solution: (a) after the electrolysis at -1.0 V (red line), after the electrolysis at -1.0 V and subsequently adding 500 equivalents of AcOH (blue line), (b) after the electrolysis at -1.5 V (red line), after the electrolysis at -1.5 V and subsequently adding 500 equivalents of AcOH (blue line), (c) after the electrolysis at -1.0 V (red line), after the electrolysis at -1.0 V and subsequently adding

40 equivalents of TFA (blue line), (d) after the electrolysis at -1.5 V (red line), after the electrolysis at -1.5 V and subsequently adding 40 equivalents of TFA (blue line), (e) after the electrolysis at -1.0 V (red line), after the electrolysis at -1.0 V and subsequently adding 40 equivalents of TsOH (blue line), (f) after the electrolysis at -1.5 V (red line), after the electrolysis at -1.5 V and subsequently adding 40 equivalents of TsOH (blue line).

Table S4 Comparison of the catalytic data for HER mediated by Cu-dbes and copper analogues

Catalyst	Medium	Proton source	Overpotential (mV)	TOF (s^{-1})	Faradaic efficiency (%)	Ref.
1	CH_3CN (0.1 M $TBAPF_6$)	AcOH TFA TsOH	550 525 520	1377 536 519	99 98 99	This work
2	CH_3CN (0.10 M [n-Bu_4N]ClO_4)	AcOH	914.6	262	-	7
3	CH_3CN (0.10 M [n-Bu_4N]ClO_4)	AcOH	914.6	220	-	7
4	DMF (0.1 M TBAP)	AcOH	130	2058.72	77.77	8
5	DMF (0.10 M [n-Bu_4N]ClO_4)	AcOH	817	457	91.5	9
6	H_2O (0.1 M KCl)	AcOH	-	49.81	-	10
7	DMF (0.1 M TBAP)	TsOH	715	138	-	11
8	CH_3CN (0.1 M TBAP)	TFA	-	356	74	12
9	CH_3CN (0.1 M TBAP)	TFA	-	227	-	12
10	CH_3CN (0.1 M TBAP)	TFA	-	49	-	12
11	DMSO (0.10 M [(n-$Bu)_4N$]ClO_4)	AcOH TFA TsOH	- - -	- - -	19.63 56.56 61.75	13
12	CH_3CN (0.1 M Bu_4NPF_6)	AcOH	230	-	-	14
13	CH_3CN (0.1 M Bu_4NPF_6)	AcOH	540	-	-	15
14	DMF (0.1 M Bu_4NPF_6)	AcOH	-	382	83	16

15	DMF (0.1 M Bu_4NPF_6)	AcOH	680	427	47	16
16	DMF (0.1 M Bu_4NPF_6)	AcOH	610	1168	89	16
17	DMF (0.1 M Bu_4NPF_6)	AcOH	710	564	50	16

$[Cu^{II}$-en-P_2(NCMe)]$(ClO_4)_2$ (en-P_2 = N,N'-bis[o-(diphenylphosphino)benzylidene]ethylenediamine) (**2**)

$[Cu^{I}$-en-$P_2]ClO_4$ (en-P_2 = N,N'-bis[o-(diphenylphosphino)benzylidene]ethylenediamine) (**3**)

[CuL] (H_2L = 1,1′-(1E,1′E)-(propane-1,2-diylbis(azan-1-yl-1-ylidene))bis(methan-1-yl-1-ylidene)dinaphthalen-2-ol) (**4**)

[CuL] (H_2L = 2,3-bis(2-hydroxybenzylideneimino)-2,3-butenedinitrile) (**5**)

[Cu(2,2′-dipyridylamine)$_2$(azide ion)]Cl ·$4H_2O$ (**6**)

[Cu(5,15-bis(pentafluorophenyl)-10-[4-(1H-imidazole) phenyl]-corrole)] (**7**)

[Cu(2,3,17-Tris(trifluoromethyl)-5,10,15-tris(pentafluorophenyl)corrole)] (**8**)

[Cu(2,3,17,18-Tetrakis(trifl uoromethyl)-5,10,15-tris(pentafluorophenyl)corrole)] (**9**)

[Cu(5,10,15-tris(pentafluorophenyl)corrole)] (**10**)

[Cu(meso-5,10,15,20-tetrakis(carboxyl)porphyrin)] (**11**)

$[Cu^{II}(L^{Et})]BF_4$ (HL^{Et} (from [1 + 1] condensation of 2,2'-iminobisbenzaldehyde (dpa) and diethylenetriamine)) (**12**)

$[Cu^{II}{}_2$(bis-$L^{Et})](BF_4)_2$ (bis-HL^{Et} (from two HL^{Et} Schiff base macrocycles (prepared by 1 + 1 condensation of 2,2'-iminobisbenzaldehyde and diethylenetriamine)) (**13**)

$[Cu^{II}$ (1,10-phenanthroline-2,6-bis(phenylselanyl)phenol)] (**14**)

$[Cu^{II}$ (1,10-phenanthroline-4-methyl-2,6-bis(phenylselanyl)phenol)] (**15**)

$[Cu^{II}$ (1,10-phenanthroline- 5,5′selenobis(4-hydroxy-3-(phenylselanyl) benzaldehyde)] (**16**)

$[Cu^{II}$ (1,10-phenanthroline- 5,5′selenobis(4-hydroxy-3-(phenylselanyl)benzonitrile)] (**17**)

References

1 C. Campana, J. Kaercher, J. Chambers and V. Petricek, Processing twinned-modulated and

composite structures from CCD / CMOS images, *Acta Crystallogr. Sect. Found. Adv.*, 2014, **70**, C173–C173.

2 G. M. Sheldrick, Crystal structure refinement with *SHELXL*, *Acta Crystallogr. Sect. C Struct. Chem.*, 2015, **71**, 3–8.

3 L. J. Farrugia, *ORTEP* -3 for windows - a version of *ORTEP* -III with a graphical user interface (GUI), *J. Appl. Crystallogr.*, 1997, **30**, 565–565.

4 W. L. J. Loke, C. Hu and W. Y. Fan, Tetrahedral Cu(I) complexes as electrocatalysts for the reduction of protons to dihydrogen gas, *Eur. J. Inorg. Chem.*, 2021, **2021**, 2499–2504.

5 A. M. Appel and M. L. Helm, Determining the overpotential for a molecular electrocatalyst, *ACS Catal.*, 2014, **4**, 630–633.

6 J.-X. Hao, Z.-W. Liu, S.-Y. Xu, L.-P. Si, L.-M. Wang and H.-Y. Liu, Electrocatalytic hydrogen evolution by cobalt(III) triphenyl corrole bearing different number of trifluoromethyl groups, *Inorg. Chim. Acta*, 2024, **564**, 121967.

7 H. Yang, J. Du, C.-L. Wang and S.-Z. Zhan, Synthesis, structures, characterizations and catalytic behaviors for hydrogen evolution of copper(II) and copper(I) complexes supported by diiminodiphosphines, *Inorg. Chem. Commun.*, 2021, **130**, 108719.

8 A. Barma, M. Chakraborty, S. K. Bhattacharya and P. Roy, Mononuclear nickel and copper complexes as electrocatalyst for generation of hydrogen from acetic acid, *Inorg. Chem. Commun.*, 2023, **150**, 110521.

9 J.-P. Cao, T. Fang, L.-Z. Fu, L.-L. Zhou and S.-Z. Zhan, First mononuclear copper(II) electro-catalyst for catalyzing hydrogen evolution from acetic acid and water, *Int. J. Hydrog. Energy*, 2014, **39**, 13972–13978.

10 N. Diyali, M. Chettri, S. Saha, A. Saha, S. Kundu, D. Mondal, D. Dhak and B. Biswas, Electrocatalytic hydrogen production activity with a copper(II)-dipyridylamine complex in acidic water, *CrystEngComm*, 2023, **25**, 6837–6844.

11 L.-W. Wu, Y.-F. Yao, S.-Y. Xu, X.-Y. Cao, Y.-W. Ren, L.-P. Si and H.-Y. Liu, Electrocatalytic hydrogen evolution of transition metal (Fe, Co and Cu)–corrole complexes bearing an imidazole group, *Catalysts*, 2024, **14**, 5.

12 K. Sudhakar, A. Mahammed, Q.-C. Chen, N. Fridman, B. Tumanskii and Z. Gross, Copper complexes of CF_3 -substituted corroles for affecting redox potentials and electrocatalysis, *ACS*

Appl. Energy Mater., 2020, **3**, 2828–2836.

13 X. Qi, G. Yang, X. Guo, L. Si, H. Zhang and H. Liu, Electrocatalytic hydrogen evolution by water‐soluble cobalt (II), copper (II) and iron (III) *meso*-tetrakis(carboxyl)porphyrin, *Eur. J. Inorg. Chem.*, 2023, **26**, e202200613.

14 A. M. Abudayyeh, O. Schott, H. L. C. Feltham, G. S. Hanan and S. Brooker, Copper catalysts for photo- and electro-catalytic hydrogen production, *Inorg. Chem. Front.*, 2021, **8**, 1015–1029.

15 V. Singh, A. M. Abudayyeh, M. G. Robb and S. Brooker, Mono-copper far more active than analogous di-copper complex for electrocatalytic hydrogen evolution, *Dalton Trans.*, 2022, **51**, 4166–4172.

16 A. Upadhyay, H. Meena, R. K. Jha, Kanika and S. Kumar, Isolation of monomeric copper(II) phenolate selenoether complexes using chelating *ortho* -bisphenylselenide-phenolate ligands and their electrocatalytic hydrogen gas evolution activity, *Dalton Trans.*, 2022, **51**, 7284–7293.